A melanocyte-melanoma precursor niche in sweat glands of volar skin(Dissertation_全文)

AUTHOR(S):

Okamoto, Natsuko

CITATION:

Okamoto, Natsuko. A melanocyte-melanoma precursor niche in sweat glands of volar skin. 京都大学, 2015, 博士(医学)

ISSUE DATE:

2015-01-23

URL:

https://doi.org/10.14989/doctor.r12890

PIGMENT CELL & MELANOMA Research

A MELANOCYTE-MELANOMA PRECURSOR NICHE IN SWEAT GLANDS OF VOLAR SKIN

Journal:	*Pigment Cell & Melanoma Research*
Manuscript ID:	14-O-148.R1
Manuscript Type:	Original Article
Date Submitted by the Author:	18-Jul-2014
Complete List of Authors:	Okamoto, Natsuko; Kyoto University Graduate School of Medicine, Department of Dermatology Aoto, Takahiro; Tokyo Medical and Dental University, Stem Cell Biology Uhara, Hisashi; Shinshu University School of Medicine, Department of Dermatology Yamazaki, Satoshi; Center for Stem Cell Biology and Medicine, Institute of Medical Science, University of Tokyo, Division of Stem Cell Therapy Akutsu, Hidenori; National Research Institute for Child Health and Development, Department of Reproductive Biology Umezawa, Akihiro; National Research Institute for Child Health and Development, Department of Reproductive Biology Nakauchi, Hiromitsu; Center for Stem Cell Biology and Medicine, Institute of Medical Science, University of Tokyo, Division of Stem Cell Therapy Miyachi, Yoshiki; Kyoto University Graduate School of Medicine, Department of Dermatology Saida, Toshiaki; Shinshu University School of Medicine, Department of Dermatology Nishimura, Emi; Tokyo Medical and Dental University, Stem Cell Biology
Keywords:	melanocyte stem cell, melanoma, sweat gland

A MELANOCYTE-MELANOMA PRECURSOR NICHE IN SWEAT GLANDS OF VOLAR SKIN

Natsuko Okamoto[2]*, Takahiro Aoto[1]*, Hisashi Uhara[4], Satoshi Yamazaki[5], Hidenori Akutsu[3], Akihiro Umezawa[3], Hiromitsu Nakauchi[5], Yoshiki Miyachi[2], Toshiaki Saida[4], Emi K. Nishimura[1]

[1]Department of Stem Cell Biology, Medical Research Institute, Tokyo Medical and Dental University, Tokyo, Japan, [2]Department of Dermatology, Kyoto University Graduate School of Medicine, Kyoto, Japan, [3]Department of Reproductive Biology, National Research Institute for Child Health and Development, Tokyo, Japan [4]Department of Dermatology, Shinshu University School of Medicine, Matsumoto, Japan, [5]Division of Stem Cell Therapy, Center for Stem Cell Biology and Medicine, Institute of Medical Science, University of Tokyo

* These authors contributed equally to this work.

Summary

Determination of the niche for early-stage cancer remains a challenging issue. Melanoma is an aggressive cancer of the melanocyte lineage. Early melanoma cells are often found in the epidermis around sweat ducts of human volar skin and the skin pigmentation pattern is an early diagnostic sign of acral melanoma. However, the niche for melanoma precursors has not been determined yet. Here we report that the secretory portion (SP) of eccrine sweat glands provide an anatomical niche for melanocyte-melanoma precursor cells. Using lineage-tagged H2B-GFP reporter mice, we found that melanoblasts which colonize sweat glands during development are maintained in an immature, slow-cycling state but renew themselves in response to genomic stress and provide their differentiating progeny to the epidermis. FISH analysis of human acral melanoma expanding in the epidermis revealed that unpigmented melanoblasts with significant CyclinD1 gene amplification reside deep in the SP of particular sweat gland(s). These findings indicate that sweat glands maintain melanocyte-melanoma precursors in an immature state in the niche and explains the preferential distribution of early melanoma cells around sweat glands in human volar skin.

Signifacance

Acral volar skin, which lacks hair follicles but contains abundant eccrine sweat glands, is highly susceptible to melanoma even without exposure to ultraviolet light. The dermoscopic pattern of parallel ridges has 99% specificity to detect acral melanomas, while the cause of the skin pigmentation pattern has been unknown. Our study is the first to identify sweat glands as the anatomical niche for melanocyte-melanoma precursor cells in mammalian volar skin.

Introduction

Human cutaneous melanoma is a highly aggressive cancer that is resistant to traditional cancer treatments (Garbe et al., 2011; Mocellin et al., 2010; Wheatley, 2003). Acral (volar skin) melanoma is the most prevalent subtype of melanoma in the non-Caucasian population. Human volar skin of peripheral extremities is minimally exposed to UV sunlight and contains abundant eccrine sweat glands but no hair follicles as the main skin appendage (Curtin et al., 2005). The characteristic skin pigmentation pattern of acral melanoma can be recognized with a magnifying glass called a dermoscopy in a "parallel ridge pattern", which reflects the preferential proliferation and differentiation of melanoma cells around sweat ducts (Oguchi et al., 1998; Saida, 2007; Saida et al., 2011; Saida et al., 2004). This method devised by Saida, one of the authors of this manuscript and his colleagues has enabled the accurate diagnosis with a 99% specificity(Saida et al., 2004) of early acral melanoma even as small as a few mm and has become the standard methodology for early diagnosis of melanoma in the volar skin nowadays. However, the origin of acral melanoma cells, the cause of the parallel ridge pattern and even the existence of melanocytic cells in sweat glands have yet to be characterized. Recent reports on sweat gland-centric distribution of melanoma cells in some acral melanoma cases(Zembowicz and Kafanas, 2012) and repigmentation of the human white spot epidermis around sweat glands(Makino et al., 2013) have suggested the possibility that unknown melanocyte precursors (melanoblasts) exist in sweat glands. Thus the skin appendage may provide a niche or special microenvironment not only for melanoblasts but also for earliest melanoma cells.

In most somatic stem cell systems, stem cells are maintained in an immature and quiescent state but become activated to undergo self-renewal to provide amplifying and differentiating progeny for tissue homeostasis (Fuchs et al., 2004; Li and Clevers, 2010). We previously identified melanocyte stem cells (McSCs) in the bulge/sub-bulge area of murine and human hair follicles and reported that the niche plays a dominant role in stem cell fate determination (Nishimura et al., 2005; Nishimura et al., 2002). The McSCs self-renew and provide their progeny not only to the hair bulb for hair pigmentation in physiological condition but also to the surrounding epidermis for skin pigmentation(Nishimura et al., 2002). During the process of epidermal repigmentation, the repigmented spots often start from the orifice of hair follicles with contiguous distribution of melanoblasts/melanocytes in the upper outer root sheath starting from the hair follicle bulge to the epidermal basal layer (Nishimura, 2011; Nishimura et al., 2002). It is thus possible that sweat glands also provide similar niche

microenvironment not only for normal melanoblasts but also for early melanoma cells.

In this paper, we hypothesized that dormant immature melanocyte-melanoma precursors exist in mammalian eccrine sweat glands which are abundantly distributed on the volar skin. We searched for the population by taking advantage of stable lineage–tagging system and we report here that such melanocyte-melanoma precursors exist in sweat glands of mammalian volar skin.

Results

To compare the architecture and pigmentation pattern of human and mouse volar skin, we first performed histological analysis. As shown in Figure 1A-C, both human and mouse volar skin were characterized by a similar thickened epidermis with rete ridges extending into the underlying dermis and by the abundant presence of sweat glands(Figure 1A-C). No pigment-containing cells or melanocytic marker-expressing cells were detectable with conventional immunohistochemistry in the sweat glands found in the footpads of non-aged adult C57/BL6Cr mice (Figure 1D). In contrast, some pigment-containing cells were found in the sweat glands and the overlying epidermis from two-year-old, aged mice (Figure 1E and data not shown), which suggested that unpigmented melanoblasts which correspond to melanocyte stem cells or progenitors exist in non-hair-bearing volar skin. *Dct-lacZ* transgene (Figure 1F) and endogenous Dct protein expression, which has been used for melanocyte lineage tagging including melanocyte stem cells (McSCs) in hair follicles (Mackenzie et al., 1997; Nishimura et al., 2002), failed to tag that cell population in adult footpad skin (Figure 1H and data not shown). Thus, we examined the developmental process of melanocytes in the distal hindlimb using Dct-lacZ and expression of endogenous Dct as markers for melanoblasts. As shown in Figure 1G and Suppl. Fig. 1-3, we succeeded in chronologically analyzing the distribution of migrating melanoblasts which first appear in the developing dermis, then in the epidermis and finally in the sweat buds, and of their eventual colonization in mature sweat glands in volar skin. This suggested that melanoblasts which colonize the sweat glands during development are maintained in a dormant and immature state with profound down-regulation of lineage markers after development until they are reactivated during the physiological aging process.

Follicular McSCs, which reside in the bulge/sub-bulge area of hair follicles, are maintained in a quiescent, inactivated state during the hair cycle except for their activation for their self-renewal at the anagen growth phase(Nishimura et al., 2005; Nishimura et al., 2002; Nishimura et al., 2010). Upon genotoxic stress or aging, the follicular McSCs ectopically differentiate within the stem cell niche without renewing themselves(Inomata et al., 2009). We hypothesized that dormant immature melanoblasts which respond to aging and/or genotoxic stress exist in the sweat glands and generate mature melanocytes. To test this, we irradiated young *Dct-lacZ* transgenic mice and searched for melanocytic cells in mouse volar skin. Melanin-containing mature melanocytes appeared in sweat glands of the mouse volar skin within a week after 5 Gy ionizing irradiation (IR) (Figure 1K) and persisted

for more than a month (Figure 1L, M), while those cells were only occasionally found in non-irradiated control skin (data not shown). As DNA damage accumulates in long-lived stem cells during aging(Nijnik et al., 2007; Rossi et al., 2007; Ruzankina et al., 2007), the above phenomenon induced by IR and the similar phenomenon associated with aging (shown in Figure 1E and I) suggest that both aging and genotoxic stress stimulate a putative stem/precursor cell population to supply pigment-producing melanocytes to the epidermis through the derma-epidermal ducts in acral volar skin.

To identify putative stem/precursor cells which would explain the above phenomena, we developed *Dct-H2B-GFP* transgenic mice, in which non-dividing/slow-cycling melanocytic cells stably retain the expression of Histone-GFP fusion protein under control of the *Dct* promoter with the LCR element once the promoter is activated (Figure 1N and Suppl. Fig. 4A)(Ganss et al., 1994; Kanda et al., 1998; Mackenzie et al., 1997). As shown in Suppl. Fig. 4B-Y, all known melanocyte lineage cells can be efficiently tagged using GFP in these transgenic mice. The distribution pattern of GFP expressing cells was identical with that of *lacZ* expressing cells in *Dct-lacZ* transgenic mice during development (Suppl. Fig. 4B-J). In mouse volar skin, GFP^+ melanoblasts appear in the epidermis by embryonic day (E) 17.5 (Figure 1O and U), then migrate down into the epidermal buds and finally colonize the tip of immature sweat glands (Figure 1P-R, U). That area then develops into the secretory portion (SP) of the sweat gland (Figure 1S, T, U). Similar migration processes were observed with *Dct-lacZ* transgenic mice (data not shown).

To identify the population which just colonizes the SP of sweat glands, we analyzed footpads of neonatal mice. The GFP^+ melanoblasts in sweat glands are located well inside the basement membrane and are surrounded by $K8^+$ luminal keratinocytes and underlying SMA^+K5^+ myoepithelial cells (Figure 2A, B, C). These GFP^+ cells in the neonatal skin express melanocyte lineage marker proteins such as MITF and Pax3 (Figure.2I, K) and downstream target genes of Mitf including Dct, Trp1 (tyrosinase-related protein 1), Tyr (tyrosinase) and Silv/Pmel17 (Figure 2D-F and data not shown), but none of the following non-melanogenic cell markers tested including Nestin (a neural progenitor marker), p75 (a neural crest progenitor marker), TuJ1 and Pgp9.5 (a peripheral nerve marker), GFAP and MPZ (Schwann cell markers) and keratin 20 (a Merkel cell marker) (Figure 2G, H, Suppl. Fig. 2 and data not shown). Furthermore, no significantly close association between these GFP^+ melanoblasts which express melanogenic genes including Dct protein during development with $TuJ1^+$ non-melanocytic cells in the dermis has been found during the earlier developmental processes as well (Suppl. Fig. 1-3 and data not shown). These data indicate

that GFP$^+$ cells which migrated from the epidermis into the developing sweat glands are melanocyte lineage cells.

Next, we examined the transition of the GFP$^+$ cell state after the neonatal stage. GFP$^+$ melanoblasts are maintained in an immature unpigmented state in the SP with drastic down-regulated expression of global melanogenic genes including Pax3 and Mitf and its downstream genes such as Dct, Dct-lacZ and Tyr by 7 weeks after development without differentiating into mature melanocytes (Figure 2I-N). At the same time, they lose expression of Mcm2, a marker for the non-Go cell state(Kingsbury et al., 2005) after the neonatal stage, indicating that these cells go into the quiescent inactivated state after development (Figure 2O, P). It is notable that McSCs which reside in the hair follicle bulge also down-regulate expression of Dct-lacZ and melanogenic genes when they enter the quiescent state(Nishimura et al., 2010) while maintaining high levels of GFP expression throughout the hair cycle (Suppl. Fig. 4 and data not shown). Thus, we concluded that melanoblasts are maintained in an immature inactivated state in the lower sweat glands after development similarly to McSCs in the hair follicle bulge area.

The other GFP$^+$ population distinguished from the melanocyte lineage in acral volar skin is the TuJ1-expressing GFP$^+$ cell population in the dermis outside of sweat glands (Figure 2G, arrowhead). Most of these cells appear at around prenatal stage in the dermis (data not shown) and coexpress the neuronal markers TuJ1 and less frequently Pgp9.5 but not Nestin, mature Schwann cell markers such as GFAP and MPZ/P0 nor the neural crest progenitor marker, p75 (Figure 2G, H, Suppl. Fig. 5 and data not shown). To confirm the identity of these dermal GFP$^+$ cells, we performed sciatic denervation. As shown in Figure 2Q and 2R, the GFP$^+$TuJ1$^+$ cells disappeared from the dermis, suggesting that the dermal GFP$^+$ cells are peripheral neurons or associated neuron-dependent precursor cells (Figure 2Q-R and Suppl. Fig.6). Then, we analyzed *Mitf*$^{ce/ce}$ mutant mice which specifically lack melanocyte lineage cells(Steingrimsson et al., 1994; Zimring et al., 1996). We found that *Mitf*$^{ce/ce}$ mice with the GFP reporter transgene lack GFP$^+$ cells in the sweat glands (Figure 2S-Y). On the other hand, TuJ1$^+$GFP$^+$ cells are maintained in the dermis with neuronal morphology in *Mitf*$^{ce/ce}$ mice as well, demonstrating that the GFP$^+$ cells in the dermis are non-melanocytic cells. To further confirm the lineage identity of GFP$^+$ cells in the sweat glands, we took advantage of ACK2, a neutralizing antibody against Kit (c-Kit), which has been used to deplete amplifying melanoblasts in developing skin(Nishimura et al., 2002). ACK2 treatment of the neonatal skin depleted almost all GFP$^+$ cells in sweat glands (Figure 3A-B and Suppl. Fig. 7), while ACK2 treatment after the neonatal stage, such as 7 weeks

after birth, did not deplete GFP$^+$ cells in the sweat glands (Figure 3B). This demonstrates that the glandular GFP$^+$ cells are *bona fide* melanoblasts which develop in Kit-dependent manner but become inactivated to go into the quiescent and immature state after the neonatal stage and survive in a Kit-independent manner similarly to slow-cycling McSCs in hair follicles(Nishimura et al., 2002).

Self-renewal and quiescence are important features of somatic stem cells including hair follicle McSCs(Cotsarelis et al., 1990; Fuchs et al., 2004; Nishimura et al., 2002). To examine whether the GFP$^+$ cells identified here are slow-cycling cells or quiescent cells, we performed pulse-chase experiments with BrdU using our transgenic mice. As shown in Figure 3C-D, we found that GFP$^+$ cells in sweat glands are able to retain the BrdU label for more than a month, while most other cells in volar skin lost their BrdU label earlier. The BrdU retention level was stably high in the majority of GFP$^+$ melanoblasts at P25 but became steadily diluted in a subset of them at P50 and was further diluted to barely detectable levels at P100 (Figure 3C-D and Suppl. Fig. 8). Adjacent GFP$^+$ cells, which show an almost identical dilution level, were also found at P50 (7wo) and show unpigmented immature cell bodies (Suppl. Fig. 8). Only a few GFP$^+$ unpigmented cells reside in the SP in each footpad (Figure 3D) and maintained well from the neonatal to the adult stage (Figure 3C). Most of these GFP$^+$ unpigmented melanoblasts are usually negative for the non-Go cell state marker Mcm2 and Ki67 after development (Figure 2O, 2P and data not shown). Therefore, these data collectively indicate that the GFP$^+$ immature melanoblasts are an extremely rare population in tissues and are normally kept in a quiescent state after development but occasionally undergo self-renewal in the SP of the sweat glands even under normal physiological conditions. As mice which congenitally lack melanocyte lineage cells (Cable et al., 1995) are able to sweat from the footpads (Suppl. Fig.9) and maintain the integrity of sweat glands (Figure 2S-X and data not shown), we assumed that the glandular melanoblasts in the SP may not be essential for the homeostasis and sweating function of sweat glands but could become pathogenic when abnormally activated.

We then determined whether the quiescent GFP$^+$ cells were able to generate pigmented melanocytes upon activation. As aged sweat glands occasionally contain pigmented melanocytes with γ-H2AX foci formation outside of the niche (data not shown), we hypothesized that melanocyte precursors are transiently activated to respond to endogenous or exogenous genomic stress during aging. To test this, we performed chronological analysis for the fate of GFP$^+$ melanoblasts after 5 Gy IR. GFP$^+$ cells in the SP

showed transient expression of Mcm2, a marker for the non-Go state (Kingsbury et al., 2005) (13.3 ± 4.7% in irradiated mice vs 0% of control mice [n=3]) (Figure 4A) and melanogenic genes such as Trp1 (6.3±4.5 % in irradiated mice vs 0% of control mice [n=3]) at 48 hr after IR (Figure 4B). Subsequently, GFP^+ pigmented melanocytes appeared within the sweat ducts of a particular gland(s) and then in the surrounding epidermis within a week after IR (Figure 4G, H, I, W, and X) while the unpigmented GFP^+ cells were maintained in the SP (Figure 4C, F, G, J, and W). Importantly, the GFP^+ cells in the SP went back to the quiescent state with down-regulation of these genes within a few days and were maintained again in an immature, unpigmented state within the niche (Figure 4J, 4P, and 4V). Those stem/precursor cell progeny generate melanin pigment by expressing melanogenic enzymes such as Tyr which is critical for melanin pigment synthesis (Figure 4T, and 4U). As only a few GFP^+ cells reside in the SP in each footpad and are stably maintained (Figure 4W), these data indicate that the GFP^+ cells in the SP maintain themselves in an immature state and at the same time provide amplifying and differentiating progeny which migrate up into the epidermis through the sweat ducts. Therefore, the GFP^+ melanoblasts in the SP show the features of adult stem cells (Potten and Loeffler, 1990) and we named the population as McSCs in sweat glands.

As the GFP^+ McSCs reside in the SP, having direct contact with $K8^+$ luminal cells and SMA^+ myoepithelial cells within the SP of sweat glands (Figure 2B,C), we assumed that the SP serves as the anatomical niche for McSCs. To exclude the involvement or contribution of GFP^+TuJ1^+ neuronal cell lineages for skin pigmentation, we performed sciatic denervation prior to IR. As shown in Suppl. Fig. 6, irradiated GFP^+ cells in the SP are able to maintain and renew themselves and are also able to generate differentiated progeny even in the absence of neuronal cells in the dermis. Furthermore, when GFP^+ cells in the SP are depleted by administration of ACK2 at the neonatal stage, mature pigmented melanocytes did not appear in the sweat glands or in the epidermis of adult acral skin even after 5 Gy IR (Figure 4X, Suppl. Fig.7, and data not shown), underlining the regenerating capability of the McSCs and their contribution to skin pigmentation.

Oncogenic stimuli such as exposure to carcinogens/mutagens and genetic alterations involved in human melanoma induce melanoma formation in mice(Larue and Beermann, 2007; Walker et al., 2011). We tested whether carcinogens also activate McSC-like precursor cells. As shown in Figure 4Y, DMBA application on mouse footpads also induced the appearance of pigmented GFP^+ cells in sweat glands. These data clearly demonstrate that MsSCs provide their pigmented progeny with the upper sweat glands in response to oncogenic or other genotoxic stimuli.

We searched for a similar McSC-like population in human acral volar skin using immunohistochemical staining with increased sensitivity (Suppl. Fig. 10). As shown in Figure 5, we detected MART1$^+$ unpigmented melanoblasts, which are located specifically in the SP of human sweat glands (Figure 5C and Suppl. Fig. 11C and 11F). Expression of other melanogenic genes (Suppl. Fig. 12 and 13) and MCM2 were not detectable in those cells in the adult skin (Figure 5C and data not shown). We also searched for a similar population in the sweat glands of non-volar skin areas such as the face and abdomen, but such melanoblasts were undetectable in those areas (data not shown). These data indicate that the population resides preferentially in the sweat glands of volar skin, at least in physiological conditions, and these immature and quiescent melanoblasts are most likely to be human McSC-like precursor cells.

Human acral skin forms a ridge and furrow pattern on the surface. Early acral melanoma shows preferential proliferation/pigmentation in the "ridge epidermis", which corresponds to crista profunda intermedia (CPI) situated under the surface ridge and contains sweat ducts in the middle of the CPI in human acral epidermis. To address the possibility that human melanoma precursors reside in the sweat glands of acral skin, we selected cases in which the skin sections cover the whole sweat gland structure and analyzed the distribution of melanocyte lineage cells in human acral melanoma (n=5) and in normal skin (n=3). We found that MART1$^+$ unpigmented melanoblasts in the SP are increased in number with co-expression of MCM2 in the specific sweat gland(s) of the melanoma *in situ* lesion, which suggests that the McSC-like cells in those particular sweat glands are renewing themselves. These MART1$^+$ proliferating cells are found in the duct as well which connects the SP to the "ridge epidermis" of the lesional epidermis (Figure 5D-F, 5M samples D-F), suggesting that MART1$^+$ cells in the SP are providing melanocytic progeny to the duct and the epidermis similarly to mouse activated McSCl progeny. Notably, these lower-positioned MART1$^+$MCM2$^+$ cells in the SP and the lower duct are unpigmented, relatively small and bipolar in morphology (Figure 5F), while those located in the upper duct or in the lesional epidermis are larger, dendritic and often pigmented (Figure 5D,E). This suggests that these abnormally proliferating cells in the lower part of sweat glands are maintained in an immature state in the special microenvironment but keep providing amplifying and differentiating melanoma cells to the epidermis. Importantly, MART1$^+$MCM2$^+$ cells are distributed contiguously or sparsely from the SP to the ridge epidermis only in particular sweat gland(s) but not in other surrounding glands in the lesion

(Figure 5D-L). We examined 10 serial sections for each early melanoma originally evaluated as melanoma *in situ* (Figure 5M, samples D-F) and more advanced melanoma (samples G and H). Each case of early acral melanoma possesses at least one sweat gland which contains proliferating $MART1^+$ cells distributed in the sweat gland starting from the SP to the intra-epidermal duct within the lesion (Figure 5D-F and 5M). Though it is believed that the distribution of early acral melanoma cells is limited within the epidermis ("*in situ*"), we found their scattered or contiguous distribution in some sweat glands. Importantly, the SP and the duct of other surrounding sweat glands are often not colonized by $MART1^+MCM2^+$ cells. Considering the features of mouse sweat gland McSCs, these findings suggest that human sweat gland melanocyte precursors are also only transiently activated for their renewal upon a stress but are able to generate abnormal melanocyte-melanoma precursors which keep proliferating in the niche in a particular or some sweat glands during aging. As the structure of those sweat glands is well maintained, the cycling precursors in the SP are most likely to keep generating their amplifying progeny which migrate toward the epidermis where they mature into histologically recognizable melanoma cells and spread horizontally within the epidermis with some colonization preference to the ridge epidermis in early acral melanoma (Suppl. Fig. 14).

CCND1 gene amplification has been found in 23.8-44.4% of early acral melanoma cases (North et al., 2008; Sauter et al., 2002; Takata et al., 2005), yet the exact distribution of the *CCND1*-amplified melanoma cells in the volar skin has not been studied. We thus tested the distribution of *CCND1*-amplified cells in the lesional skin by DNA-FISH analysis. As shown in Figure 6A, *CCND1*-amplified cells were found in the SP in multiple cases of early acral melanoma which were originally evaluated as melanoma in situ (n=3/4 cases) with their contiguous distribution along the duct up to the epidermis. It is notable that the *CCND1* amplification level in melanoma cells is significantly higher in the epidermis than in the SP (Figure 6B and data not shown). The opposite pattern (less amplification in the epidermis) has not been found in any acral melanoma cases examined. The significant increase of *CCND1* gene amplification level in the epidermis indicates that melanoma cells in the SP not only maintain themselves in an immature unpigmented state in particular gland(s) but also can provide their amplifying progeny which then undergo more amplification in the epidermis. We thus concluded that the SP of acral sweat glands serves as the reservoir of early melanoma precursors which can generate noticeably mature melanoma cells with more oncogenic alterrations and expansion in the epidermis (Figure 6C).

Discussion

In this study, we identified McSCs s, which possess somatic stem cell characteristics, in sweat glands in murine volar skin. We found that the SP of the sweat glands are the anatomical niche not only for those melanoblasts but also for early human melanoma precursors with *CCND1* gene amplification. As far as we know, this is the first identification of the niche for oncogenically mutated early cancer cells in human solid cancer tissues, while leukemogenic mutations such as *BCR-ABL* mutations have been found in hematopoietic stem cells(Rossi et al., 2008), the exact niche for early cancer cells remain unknown even in solid cancer as far as we know. Visually detectable pigmentation of the earliest melanoma *in situ* lesions such as those with a few mm in diameter is the suitable system to tackle this problem and allowed us to search for the niche where melanoblsts with early genetic melanoma alteration are hiding deep in the skin.

McSCs in sweat glands are an extremely rare population in the skin compared to McSCs in hair follicles and are more resistant to X-ray, but possess many similar stem cell characteristics. They are normally immature and slow-cycling but transiently renew-themselves not only physiologically but also in response to genotoxic stress and provide an amplifying and differentiating progeny into the epidermis through the ascending sweat duct which connect the SP to the epidermis. As those McSCs are maintained in an immature and quiescent state in the SP, where sweat gland keratinocytes are also maintained in a quiescent state (Lu et al., 2012; Nakamura and Tokura, 2009), both in mice and in humans, the SP seems to provide a special niche microenvironment for a fixed number of McSC-like cells in an inactivated immature state (shown schematically in Figure 6C scheme). In contrast, immature but amplifying McSC-like cells or immature melanoma precursor cells in human volar skin were found in the SP of particular sweat glands of early acral melanoma lesions. As these McSC-like cells do not form a tumor mass within the SP but amplifying and differentiating melanoma cells are distributed in the upper area of the gland(s) and the surrounding epidermis, it is most likely that mutated McSC-like cells in the SP keep providing their amplifying and differentiating progeny toward the epidermis as tumor-initiating cells or cancer stem cells. The melanoma cell distribution pattern, the *CCND1* amplification pattern in the SP vs. in the epidermis of those early melanoma cases and the immaturity of those melanoma cells in the SP collectively suggest that the McSC-like

cells in the SP are the initial origin of human acral melanoma at least in some cases. As copy number amplification requires the DNA replication process(Hastings et al., 2009), it is most likely that these mutated McSC-like cells in the SP of particular sweat gland(s) generate more amplified subclones which expand for further progression outside of their niche mainly in the epidermis during early melanomagenesis. The origin of melanoma cells, thus, may explain the preferential proliferation and pigmentation of acral melanoma cells in the CPI around epidermal ducts. However, our data do not exclude the possibility that some acral melanomas also originate directly from epidermal melanocytes and migrate down to the SP of some sweat glands to colonize the niche and become unpigmented and obtain the immature property common to McSCs upon their colonization of the SP (Figure.6C and Suppl. Fig.14). Recently reported melanoma variant called "syringotropic melanoma", which shows the prominent involvement of sweat glands (Zembowicz and Kafanas, 2012) may represent one of the two possibilities. The radial distribution pattern of melanoma cells from the sweat glands suggest that melanoma cells can be originated from McSC-like cells in the SP of sweat glands but further studies are necessary. In either case, our data indicated that sweat glands provide an anatomical niche not only for normal McSC-like cells but also for early melanoma cells in the volar skin and suggested that renewing melanoma cells with early genetic alteration (s) in the SP can further evolve into subclones with more genetic alterations within the epidermis.

Moreover, the fact that acral McSC-like cells are activated to renew themselves upon genomic stress such as IR may explain the IR-refractory characteristics and genomic instability frequently found in early acral melanoma(Curtin et al., 2005). As amplifying McSC-like cells or melanoma precursors with an oncogenic mutation reside in the SP located deep in the subcutaneous fat, sufficient deep surgical excision of the niche lesion and accurate staging of acral melanoma with careful evaluation of tumor depth and involvement of McSC-like melanoma precursors may improve the prognosis of melanoma patients. Further studies on the melanocyte precursors as a melanoma origin or tumor-initiating cells, their topographical dynamics for clonal evolution and their potential for therapeutic target are necessary to combat this devastating cancer.

METHODS SUMMARY

See Supplementary Information for detailed methods.

Mice:

Dct-H2B-GFP mice were newly generated as described in Supplementary Information. *Dct-LacZ* transgenic mice were a kind gift from Dr. Ian Jackson. *MITF-ce* mice were a kind gift from Dr. M. Lynn Lamoreux(Zimring et al., 1996).

BrdU injection:

Mice were injected subcutaneously at 24 hr intervals with 20 µl BrdU solution in PBS at 2 mg ml^{-1}.

ACK2 treatment

For the treatment of neonatal mice, 200 µg ACK2 was injected into the peritoneal cavity at days 0, 2 and 4 after birth(Nishimura et al., 2002). For the treatment of adult mice, 1 mg ACK2 was injected into the peritoneal cavity at the days 1, 3, 5, 7 and 9 after plucking at P49.

Irradiation:

Mice were irradiated at a dose of 5 Gy using 1.0 mm Aluminum filters as previously described (Inomata et al., 2009)

Histology

Immunohistochemistry was performed as previously described (Inomata et al., 2009).

References

Cable, J., Jackson, I. J., and Steel, K. P. (1995). Mutations at the W locus affect survival of neural crest-derived melanocytes in the mouse. Mech Dev *50*, 139-50.

Cotsarelis, G., Sun, T.-T., and Lavker, R. M. (1990). Label-retaining cells reside in the bulge area of pilosebaceous unit: Implications for follicular stem cells, hair cycle, and skin carcinogenesis. Cell *61*, 1329-1337.

Curtin, J. A., Fridlyand, J., Kageshita, T., Patel, H. N., Busam, K. J., Kutzner, H., Cho, K.-H., Aiba, S., Bröcker, E.-B., Leboit, P. E., et al. (2005). Distinct Sets of Genetic Alterations in Melanoma. New England Journal of Medicine *353*, 2135-2147.

Fuchs, E., Tumbar, T., and Guasch, G. (2004). Socializing with the Neighbors: Stem Cells and Their Niche. Cell *116*, 769-778.

Ganss, R., Montoliu, L., Monaghan, A. P., and Schutz, G. (1994). A cell-specific enhancer far upstream of the mouse tyrosinase gene confers high level and copy number-related expression in transgenic mice. EMBO J *13*, 3083-93.

Garbe, C., Eigentler, T. K., Keilholz, U., Hauschild, A., and Kirkwood, J. M. (2011). Systematic Review of Medical Treatment in Melanoma: Current Status and Future Prospects. The Oncologist *16*, 5-24.

Hastings, P. J., Lupski, J. R., Rosenberg, S. M., and Ira, G. (2009). Mechanisms of change in gene copy number. Nat Rev Genet *10*, 551-564.

Inomata, K., Aoto, T., Binh, N. T., Okamoto, N., Tanimura, S., Wakayama, T., Iseki, S., Hara, E., Masunaga, T., Shimizu, H., et al. (2009). Genotoxic Stress Abrogates Renewal of Melanocyte Stem Cells by Triggering Their Differentiation. Cell *137*, 1088-1099.

Kanda, T., Sullivan, K. F., and Wahl, G. M. (1998). Histone-GFP fusion protein enables sensitive analysis of chromosome dynamics in living mammalian cells. Curr Biol *8*, 377-85.

Kingsbury, S. R., Loddo, M., Fanshawe, T., Obermann, E. C., Prevost, A. T., Stoeber, K., and Williams, G. H. (2005). Repression of DNA replication licensing in quiescence is independent of geminin and may define the cell cycle state of progenitor cells. Experimental Cell Research *309*, 56-67.

Li, L., and Clevers, H. (2010). Coexistence of Quiescent and Active Adult Stem Cells in Mammals. Science *327*, 542-545.

Lu, Catherine p., Polak, L., Rocha, Ana s., Pasolli, H. A., Chen, S.-C., Sharma, N., Blanpain, C., and Fuchs, E. (2012). Identification of Stem Cell Populations in Sweat Glands and Ducts Reveals Roles in Homeostasis and Wound Repair. Cell *150*, 136-150.

Mackenzie, M. a. F., Jordan, S. A., Budd, P. S., and Jackson, I. J. (1997). Activation of the Receptor Tyrosine Kinase Kit Is Required for the Proliferation of Melanoblasts in the Mouse Embryo. Developmental Biology *192*, 99-107.

Makino, T., Yanagihara, M., Oiso, N., Mizawa, M., and Shimizu, T. (2013). Repigmentation of the epidermis around the acrosyringium in piebald skin: an ultrastructural examination. British Journal of Dermatology *168*, 910-912.

Mocellin, S., Pasquali, S., Rossi, C. R., and Nitti, D. (2010). Interferon Alpha Adjuvant Therapy in Patients With High-Risk Melanoma: A Systematic Review and Meta-analysis. JNCI Journal of the National Cancer Institute *102*, 493-501.

Nakamura, M., and Tokura, Y. (2009). The Localization of Label-Retaining Cells in Eccrine Glands. J Invest Dermatol *129*, 2077-2078.

Nijnik, A., Woodbine, L., Marchetti, C., Dawson, S., Lambe, T., Liu, C., Rodrigues, N. P., Crockford, T. L., Cabuy, E., Vindigni, A., et al. (2007). DNA repair is limiting for haematopoietic stem cells during ageing. Nature *447*, 686-690.

Nishimura, E. K. (2011). Melanocyte stem cells: a melanocyte reservoir in hair follicles for hair and skin pigmentation. Pigment Cell & Melanoma Research *24*, 401-410.

Nishimura, E. K., Granter, S. R., and Fisher, D. E. (2005). Mechanisms of Hair Graying: Incomplete Melanocyte Stem Cell Maintenance in the Niche. Science *307*, 720-724.

Nishimura, E. K., Jordan, S. A., Oshima, H., Yoshida, H., Osawa, M., Moriyama, M., Jackson, I. J., Barrandon, Y., Miyachi, Y., and Nishikawa, S.-I. (2002). Dominant role of the niche in melanocyte stem-cell fate determination. Nature *416*, 854-860.

Nishimura, E. K., Suzuki, M., Igras, V., Du, J., Lonning, S., Miyachi, Y., Roes, J., Beermann, F., and Fisher, D. E. (2010). Key Roles for Transforming Growth Factor-beta in Melanocyte

Stem Cell Maintenance. Cell stem cell *6*, 130-140.
North, J. P., Kageshita, T., Pinkel, D., Leboit, P. E., and Bastian, B. C. (2008). Distribution and Significance of Occult Intraepidermal Tumor Cells Surrounding Primary Melanoma. J Invest Dermatol *128*, 2024-2030.
Oguchi, S., Saida, T., Koganehira, Y., Ohkubo, S., Ishihara, Y., and Kawachi, S. (1998). Characteristic Epiluminescent Microscopic Features of Early Malignant Melanoma on Glabrous Skin: A Videomicroscopic Analysis. Arch Dermatol *134*, 563-568.
Potten, C. S., and Loeffler, M. (1990). Stem cells: attributes, cycles, spirals, pitfalls and uncertainties. Lessons for and from the crypt. Development *110*, 1001-1020.
Rossi, D. J., Bryder, D., Seita, J., Nussenzweig, A., Hoeijmakers, J., and Weissman, I. L. (2007). Deficiencies in DNA damage repair limit the function of haematopoietic stem cells with age. Nature *447*, 725-729.
sRossi, D. J., Jamieson, C. H. M., and Weissman, I. L. (2008). Stems Cells and the Pathways to Aging and Cancer. Cell *132*, 681-696.
Ruzankina, Y., Pinzon-Guzman, C., Asare, A., Ong, T., Pontano, L., Cotsarelis, G., Zediak, V. P., Velez, M., Bhandoola, A., and Brown, E. J. (2007). Deletion of the Developmentally Essential Gene ATR in Adult Mice Leads to Age-Related Phenotypes and Stem Cell Loss. Cell stem cell *1*, 113-126.
Saida, T. (2007). Morphological and molecular uniqueness of acral melanoma. Expert Review of Dermatology *2*, 125-131.
Saida, T., Koga, H., and Uhara, H. (2011). Key points in dermoscopic differentiation between early acral melanoma and acral nevus. The Journal of Dermatology *38*, 25-34.
Saida, T., Miyazaki, A., Oguchi, S., Ishihara, Y., Yamazaki, Y., Murase, S., Yoshikawa, S., Tsuchida, T., Kawabata, Y., and Tamaki, K. (2004). Significance of Dermoscopic Patterns in Detecting Malignant Melanoma on Acral Volar Skin: Results of a Multicenter Study in Japan. Arch Dermatol *140*, 1233-1238.
Sauter, E. R., Yeo, U.-C., Von Stemm, A., Zhu, W., Litwin, S., Tichansky, D. S., Pistritto, G., Nesbit, M., Pinkel, D., Herlyn, M., et al. (2002). Cyclin D1 Is a Candidate Oncogene in Cutaneous Melanoma. Cancer Research *62*, 3200-3206.
Steingrimsson, E., Moore, K. J., Lamoreux, M. L., Ferre-D'amare, A. R., Burley, S. K., Zimring, D. C., Skow, L. C., Hodgkinson, C. A., Arnheiter, H., Copeland, N. G., et al. (1994). Molecular basis of mouse microphthalmia (mi) mutations helps explain their developmental and phenotypic consequences. Nat Genet *8*, 256-63.
Takata, M., Goto, Y., Ichii, N., Yamaura, M., Murata, H., Koga, H., Fujimoto, A., and Saida, T. (2005). Constitutive Activation of the Mitogen-Activated Protein Kinase Signaling Pathway in Acral Melanomas. J Investig Dermatol *125*, 318-322.
Wheatley, K. (2003). Does adjuvant interferon-α for high-risk melanoma provide a worthwhile benefit? A meta-analysis of the randomised trials. Cancer Treatment Reviews *29*, 241-252.
Zembowicz, A., and Kafanas, A. (2012). Syringotropic Melanoma: A Variant of Melanoma With Prominent Involvement of Eccrine Apparatus and Risk of Deep Dermal Invasion. The American Journal of Dermatopathology *34*, 151-156 10.1097/DAD.0b013e318227c90d.
Zimring, D. C., Lamoreux, M. L., Millichamp, N. J., and Skow, L. C. (1996). Microphthalmia cloudy-eye (mi(ce)): a new murine allele. J Hered *87*, 334-8.

Acknowledgements

We thank Dr. Ian Jackson (Roslin Institute) for the *Dct-LacZ* mice; Dr.Vincent Hearing (National Cancer Institute) for antibodies; Dr. David Fisher (Harvard Medical School) for antibodies; Dr. Shinichi Nishikawa (RIKEN C.D.B.) for plasmid; Dr. Ryuhei Okuyama (Shinsyu University) for his support; Dr. Robert Hoffman (University of California, San Diego) for his critical reading of the manuscript; Dr. Hatsune Makino (National Research Institute for Child Health and Development) for her support for human samples; Dr. Ken Inomata for his support for experiments; Dr. Hideaki Tanizaki and Dr. Hiroshi Kaku for skin excision surgery at Kyoto University. E.K.N is supported by JSPS Funding Program for Next Generation World-leading Researchers (NEXT Program) and Grant-in-Aid for Scientific Research on Innovative Areas.

Competing financial interests
The authors declare no competing financial interests.

Author Information Correspondence and requests for materials should be addressed to E. K. N (nishscm@tmd.ac.jp)

Figure Legends

Figure 1

The existence of melanocytic sources in human and mouse sweat glands of acral skin.

A, **B**, Organization of eccrine sweat glands in mouse and human acral skin. The Hematoxylin-Eosin-stained sections are from human finger skin (A) and mouse footpad skin (B). **C**, Schematic diagram of a sweat gland. The structure is similar both in mice and in humans. **D**, **E**, Hematoxylin-Eosin-stained sections of footpad skin of 7-week-old (7wo) (young) (D) and 2-year-old (2yr) (old) (E) mice). Melanin-containing cells are observed in the sweat duct, but not in the secretory portion (SP), of 2-year-old mice (arrowheads). **F**, Structure of the LacZ reporter under control of the melanocyte-specific Dct promoter (Dct-LacZ). **G-I,** LacZ-stained skin of the footpad of *Dct-LacZ* tg mice (G; 5-day-old (P5), H; 7-week–old (7wo) and I; 2-year-old (2yo)). $LacZ^+$ melanocytic cells are found in the sweat duct and SP at P5 mice (arrows) and old mice, while no $LacZ^+$ cells are detectable at 7wo (H). **J**-**L**, LacZ-stained skin of the footpad of 5 Gy-irradiated *Dct-LacZ* tg mice. Dct-$LacZ^+$ cells (arrow) appear in the sweat duct at 1 week (1wk) after IR (K) and melanin-containing cells (arrowheads) appear in the sweat duct at 4 weeks (4wk) after IR (L). J-M, stained with hematoxylin-eosin, **L, M**, Fontana-Masson staining for the detection of melanin. **N**, Structure of the H2B-GFP reporter under control of the melanocyte-specific Dct promoter and the LCR element (Dct-H2B-GFP). **O**-**T**, Distribution of H2B-GFP expressing cells in the developing footpad skin of *Dct-H2B-GFP* tg mice at different stages. GFP^+ cells migrating from the epidermis (green: arrows) towards the SP (the area encircled by the dotted line) of glands. Keratin 5^+ myoepithelial/basal keratinocyte immunostaining (red) defines the gland structure. GFP^+ cells are found in the epidermis at E17.5 (O) and subsequently in the EG primordial buds at E18.5 (P). At postnatal day (P) 1 (Q), GFP^+ cells are found in the developing ducts. The majority of GFP^+ cells are settled in the SP of glands between P5 (R), 2 weeks (2wo) (S) and 7 weeks (7wo) (T) after birth. Nuclei are counterstained with DAPI (blue). The insets show magnified images of GFP expressing cells.

Figure 2

Identification of slow-cycling melanoblasts located in the SP of sweat glands in acral skin using *Dct-H2B-GFP* transgenic (tg) mice.

A-G, Confocal analysis of GFP and immunostaining of various lineage markers performed

on P5 footpad sections of *Dct-H2B-GFP* tg mice. A, B, GFP^+ cells (green) are located between Keratin 8^+ glandular cells (red)(A) and α-SMA^+ myoepithelial cells (red)(B). GFP^+ cells in the developing SP (the area encircled by the dotted line) of glands co-express melanosomal proteins, TRP1 (C), TYR (D) and Pmel17/Silv (E**)** but not TuJ1 (F) or GFAP (G). TYR^- immature GFP^+ cells were also occasionally found in the SP (d, dotted arrow). Nuclei are counterstained with DAPI (blue). **H–O,** expression of GFP and various cell markers in the SP at P5 and 7wo. Down-regulation of the lineage markers Pax3, MITF or Dct was observed in GFP^+ melanoblasts in the SP of adult mice (H-M). GFP^+ melanoblasts were kept in an $MCM2^-$ quiescent state in the adult stage (I,K,O). **P**, **Q**, The number of GFP^+TuJ1^+ cells (arrowhead) in the dermis were profoundly reduced after sciatic denervation, while GFP^+TuJ1^- cells (arrows) were maintained in the SP. **R**,**S**, Immunostaining of the footpad sections of 7wo $MITF^{ce/+}$;$Dct\text{-}H2B\text{-}GFP^{tg/+}$ (R) and $MITF^{ce/ce}$;$Dct\text{-}H2B\text{-}GFP^{tg/+}$ (S) mice for GFP and TuJ1 expression. GFP^+TuJ1^- melanocytes (arrows) were found in the SP of $MITF^{ce/+}$ but not in $MITF^{ce/ce}$ mice. GFP^+TuJ1^+ neurons exist outside of the glands in both types of mice. **T,** The average number of GFP^+TuJ1^- melanoblasts per gland in a single footpad and per single hair follicles and the dermal GFP^+TuJ1^+ cells (per single footpad skin and per 1 mm width of dorsal skin) at 7 weeks in $MITF^{ce/+}$;$Dct\text{-}H2B\text{-}GFP^{tg/+}$ and $MITF^{ce/ce}$;$Dct\text{-}H2B\text{-}GFP^{tg/+}$ mice.

Figure 3

Dct-H2B-GFP^+ cells are slow cycling, ACK2 resistant melanoblasts in adult skin.

A-B, The differential ACK2 sensitivity of GFP^+TuJ1^- cells in sweat glands after ACK2 administration at the neonatal (A) or the adult stage (B). The number of GFP^+TuJ1^- cells in the SP is shown. A, While GFP^+TuJ1^- cells are found in the SP of control mice (green; arrows), almost no GFP^+TuJ1^- cells remain in the SP of neonatal ACK2-treated mice. B, GFP^+TuJ1^- cells remain in the SP of adult ACK2-treated mice. Error bars represent s.d. of 3 independent experiments. *, statistical significance at the level of $P < 0.01$. **C-D**, Pulse-chase experiments with BrdU in *Dct-H2B-GFP* tg mice. The total number of GFP^+TuJ1^- cells in the SP did not significantly change from post-neonatal (P10) to adult stage (7wo) (C). After continuous BrdU injection (P1-P10), almost all cells in the acral skin of *Dct-H2B-GFP* tg mice were labeled with BrdU at P10 (D; arrows (SP)). At P25 and 7wo, GFP^+ melanoblasts were found exclusively in the SP of sweat glands with significant retention of BrdU (D). The label is still retained in some

GFP$^+$ melanoblasts at 7wo (D; arrows and C). The insets show magnified images of GFP expressing cells.

Figure 4

Melanoblasts in the SP of sweat glands maintain themselves and provide proliferating and differentiating melanocytes to the epidermis in response to IR or oncogenic stress.

A-T Behavior of GFP$^+$ cells in sweat glands after 5 Gy IR. Immunostaining for keratin 5 (K5) was performed on footpad skin sections in *Dct-H2B-GFP* tg mice to chase GFP$^+$ cells (green) located within the glands after IR. While no GFP$^+$ cells exist in the duct or the epidermis in control mice (A-D), GFP$^+$ cells (arrows) exist in the dermal-epidermal duct and the epidermis after IR at 1 week (1wk) (E-H). Bright view images merged with GFP images are shown for the epidermis (solid-line square) (B, F), the sweat duct (marked by the long-dashed line square) (C, G) and SP (the short-dashed line square) (D, H) on the right side of the large panel. Melanogenesis can be observed only in the duct or in the epidermis (F, G). I-N and O-T, MCM2 and TYR immunostaining images are shown respectively on the right side of the figure. Most GFP$^+$ cells (arrows) at the SP are MCM2- (K,N), while IR-induced ductal or epidermal GFP$^+$ melanocytes (arrows) are MCM2$^+$ (red) (M,L) and TYR$^+$ (red) (R,S). **U,V**, Transient cell cycle entry and commitment of GFP$^+$ cells in the SP. At around 48 hr after IR, expression of MCM2 and TRP1 was found transiently in some GFP$^+$ cells located within the SP (arrow). **W**, The number of GFP$^+$ cells located in the SP remained stable after IR(graph in the upper column), while the number of GFP$^+$ cells located within the duct of glands after IR was significantly increased (graph in the lower column). *, statistical significance at the level of $P < 0.05$. **X**, IR-induced pigmentation of the upper portions of glands after IR was dramatically impaired when mice were pretreated with ACK2 at the neonatal stage (Z). Error bars represent s.d. of 3 independent experiments. *, statistical significance at the level of $P < 0.01$. Nuclei are counterstained with DAPI (blue). **Y**, Pigmented GFP$^+$ cells (red arrow) were found in the duct at 4 weeks after DMBA, while GFP$^+$ cells in the SP were kept in an unpigmented state.

Figure 5

Identification of melanoblasts in the SP of human volar sweat glands as an expandable source of early acral melanoma.

A-L, Localization of melanocyte/melanoma cells and their cell cycle status in human volar

sweat glands. Human normal volar skin (A-C) and early melanoma skin (D-L) were immunostained for the lineage markers, MART1 (shown in green) and MCM2 (in red). A small number of $MART1^{+}MCM2^{-}$ cells is found in the epidermis close to the sweat duct within the ridge area of the skin (A) and the SP (C) but not within the duct (B). **D,** A nest of $MART1^{+}MCM2^{+}$ unpigmented melanoma cells (white arrows) and $MART1^{+}MCM2^{low}$ pigmented melanoma cells (red arrows) was found in the epidermis of the ridge area of the lesional skin of melanoma *in situ*. $MART1^{+}$ cells are aligned contiguously throughout the duct (arrow; E) and SP (arrow; F) area of a particular sweat gland within the center of the lesion. At the periphery of the lesion, $MART1^{+}MCM2^{+}$ cells were found in the epidermis (arrow; G) but not in sweat glands (arrow; I). At the intact margin, there are $MART1^{+}MCM2^{-}$ melanoblasts but no $MART1^{+}MCM2^{+}$ cells in the epidermis (J). The SP of an identical gland contains a $MART1^{+}MCM2^{-}$ melanoblast (L). Note that $MART1^{+}$ cells were found in the duct of particular glands at the lesion but not in the surrounding glands at the margin of the lesion (H and K). Magnified images of $MART1^{+}$ cells are shown in the insets. Nuclei are counterstained with DAPI. **M,** Table showing the distribution and proliferative status of $MART1^{+}$ cells in human acral skin samples. In normal control skin samples, a small number of $MART1^{+}$ cells were found in the SP and most of them are $MCM2^{-}$, while those in early melanoma lesions are $MCM2^{+}$ and $MART1^{+}MCM2^{+}$ proliferative cells were found in the sweat duct and SP of particular glands.

Figure 6

***CCND1* gene amplification in the SP within a melanoma lesion and a schematic for McSC-like cell development, maintenance and melanomagenesis.**

A. Histograms showing the distribution of copy number variation of 11q13 *CCND1* genomic regions in the tumor center of early acral melanomas. Colored bars (red, blue, green, and yellow) show individual samples derived from acral melanoma cases, while colored bars (black and white) show control normal samples. The *Cep11* centromeric region was used to normalize FISH signals between cells at different cell cycle stages. **B.** Box plot showing the copy number differences between the epidermis and SP from melanoma and normal skin. Copy number amplification of the *CCND1* gene is found in the SP of sweat glands within the lesion but not in the normal skin, is significantly lower than that seen in the epidermis. *, statistical significance at the level of $P < 0.05$. **C**. The fate and behavior of melanocyte lineage cells in sweat glands are summarized and combined with a hypothetical schematic for melanoma initiation from McSCs. Proliferating melanoblasts (red) which colonized the SP of

the sweat glands enter a quiescent (Go) state just after development and become McSCs maintained in a dormant state (blue). These cells are activated transiently by extrinsic or intrinsic stresses such as genotoxic stress and during the normal ageing process. Conversely, the corresponding population in the SP maintains its immaturity and cycling activity to renew the population and to generate their amplifying progenies which acquire further genetic alterations during their migration and maturation into noticeable melanoma cells in the epidermis.

Supporting Information Legend List

Supplementary Figure 1
Distribution of developing melanoblasts and peripheral neurons in the distal hindlimb of mouse embryos.

Supplementary Figure 2
Migration of developing melanoblasts into the epidermis for their eventual colonization of the footpad epidermis in mice.

Supplementary Figure 3
Dct-expressing melanoblasts in sole skin do not coexpress a neural lineage marker TuJ1.

Supplementary Figure 4'
Characterization of *Dct-H2B-GFP* transgenic (tg) mice.

Supplementary Figure 5
GFP^+ cells in the sweat glands of *Dct-H2B-GFP* tg mice are distinct from $Nestin^+$ neural progenitors, $p75^+$ neural crest progenitors, $TuJ1^+$ neurons, and $GFAP^+$ Schwann cells.

Supplementary Figure 6
GFP^+ melanoblasts in the SP of sweat glands of denervated footpads provide their pigmented progenies to the epidermis after IR.

Supplementary Figure 7
Depletion of developing McSCs in acral skin eradicates the IR-induced appearance of melanocytes in sweat glands and in the epidermis.

Supplementary Figure 8
Slow-cycling GFP^+ melanoblasts exist in the SP area of sweat glands in adult acral skin under physiological conditions.

Supplementary Figure 9
Sweating response is detectable in melanocyte-deficient $Kit^{W/W\text{-}V}$ mice.

Supplementary Figure 10
Low level of MART1 is expressed by quiescent McSC-like cells in human hair follicles.

Supplementary Figure 11

Human MART1^{+} melanoblasts are located in the epidermis and SP of sweat gland in the acral skin.

Supplementary Figure 12
Expression of most melanogenic proteins is undetectable in human melanoblasts in the SP of sweat glands in infant skin.

Supplementary Figure 13
Human melanoblasts in the SP of sweat glands do not express HMB45, TYR, or Ki67 in adult skin.

Supplementary Figure 14
Hypothetical scheme of melanomagenesis in human acral skin.

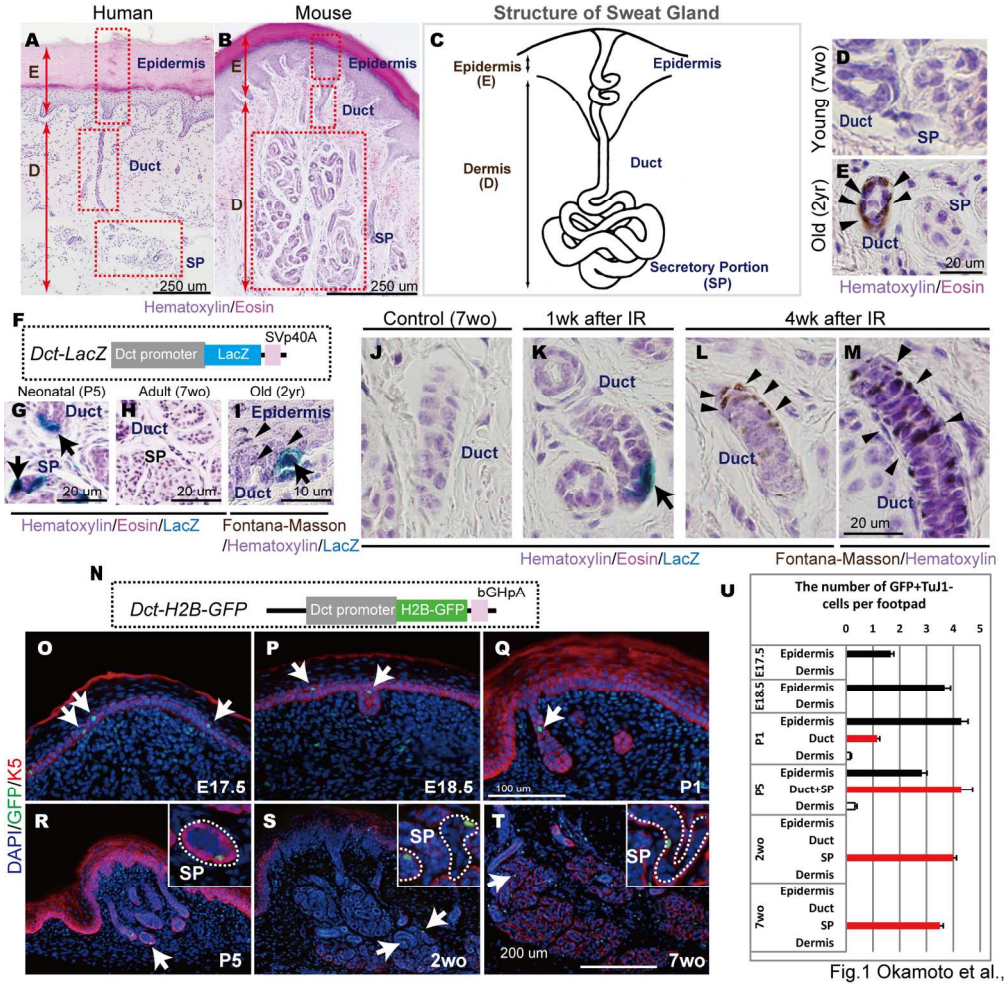

Fig.1 Okamoto et al.,

Figure 1. The existence of melanocytic sources in human and mouse sweat glands of acral skin. A, B, Organization of eccrine sweat glands in mouse and human acral skin. The Hematoxylin-Eosin-stained sections are from human finger skin (A) and mouse footpad skin (B). C, Schematic diagram of a sweat gland. The structure is similar both in mice and in humans. D, E, Hematoxylin-Eosin-stained sections of footpad skin of 7-week-old (7wo) (young) (D) and 2-year-old (2yr) (old) (E) mice). Melanin-containing cells are observed in the sweat duct, but not in the secretory portion (SP), of 2-year-old mice (arrowheads). F, Structure of the LacZ reporter under control of the melanocyte-specific Dct promoter (Dct-LacZ). G, H, LacZ-stained skin of the footpad of Dct-LacZ tg mice (G; 5-day-old (P5) and H; 7-week–old (7wo)). LacZ+ melanocytic cells are found in the sweat duct and SP at P5 mice (arrows), while no LacZ+ cells are detectable at 7wo. I-L, LacZ-stained skin of the footpad of 5 Gy-irradiated Dct-LacZ tg mice. Dct-LacZ+ cells (arrow) appear in the sweat duct at 1 week (1wk) after IR (J) and melanin-containing cells (arrowheads) appear in the sweat duct at 4 weeks (4wk) after IR (K). I-J, stained with hematoxylin-eosin, L, Fontana-Masson staining for the detection of melanin. M, Structure of the H2B-GFP reporter under control of the melanocyte-specific Dct promoter and the LCR element (Dct-H2B-GFP). N-S, Distribution of H2B-GFP expressing cells in the developing footpad skin of Dct-H2B-GFP tg mice at different stages. GFP+ cells migrating from the epidermis (green: arrows) towards the SP (the area encircled by the dotted line) of glands. Keratin 5+ myoepithelial/basal keratinocyte immunostaining (red) defines the gland structure. GFP+ cells are found in the epidermis at E17.5 (N) and subsequently in the EG primordial buds at E18.5 (O). At postnatal day (P) 1 (P), GFP+ cells are found in the developing ducts. The majority of GFP+ cells are settled in the SP of glands between P5 (Q), 2 weeks (2wo) (R) and 7 weeks (7wo) (S) after birth. Nuclei are counterstained with DAPI (blue). The insets show magnified images of GFP expressing cells.

149x146mm (300 x 300 DPI)

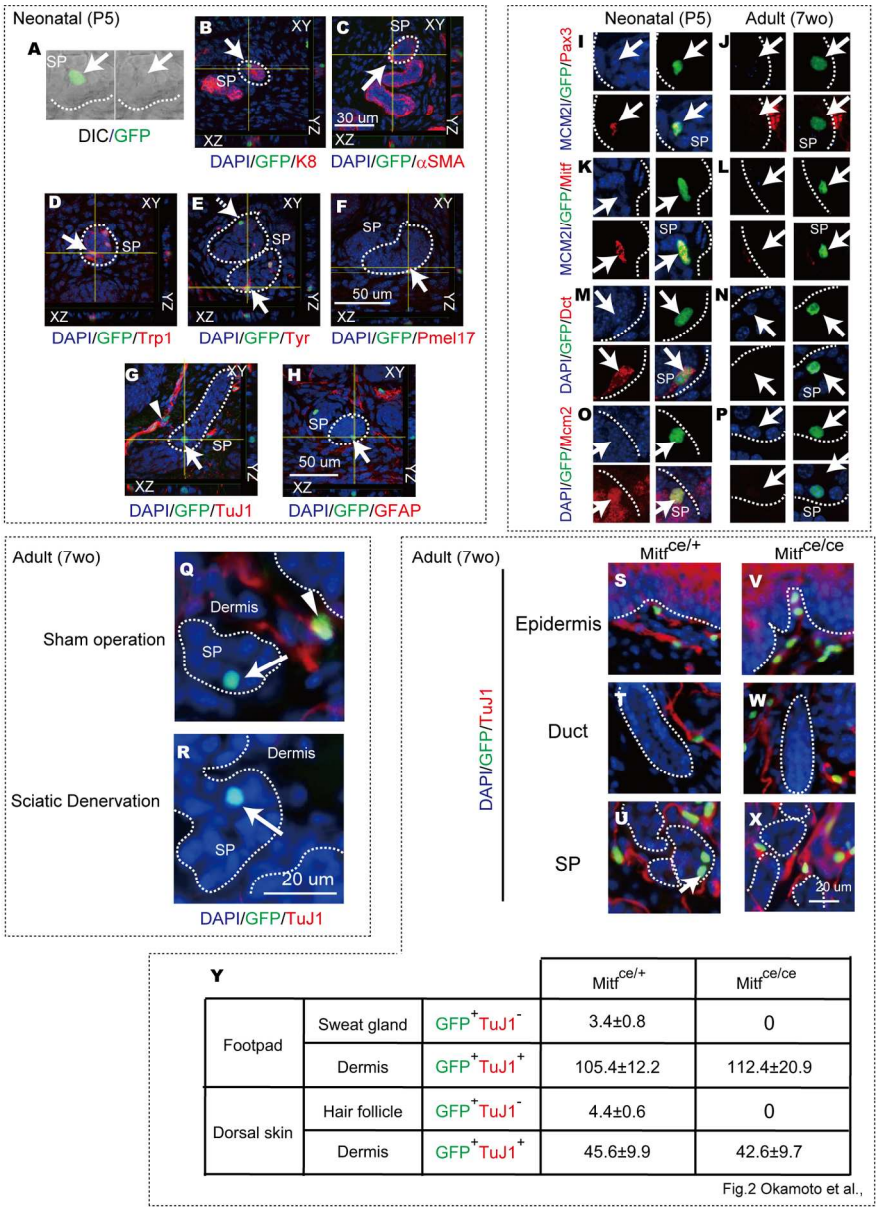

Y

			$Mitf^{ce/+}$	$Mitf^{ce/ce}$
Footpad	Sweat gland	$GFP^{+}TuJ1^{-}$	3.4±0.8	0
	Dermis	$GFP^{+}TuJ1^{+}$	105.4±12.2	112.4±20.9
Dorsal skin	Hair follicle	$GFP^{+}TuJ1^{-}$	4.4±0.6	0
	Dermis	$GFP^{+}TuJ1^{+}$	45.6±9.9	42.6±9.7

Figure 2. Identification of slow-cycling melanoblasts located in the SP of sweat glands in acral skin using Dct-H2B-GFP transgenic (tg) mice.

A-G, Confocal analysis of GFP and immunostaining of various lineage markers performed on P5 footpad sections of Dct-H2B-GFP tg mice. A, B, GFP+ cells (green) are located between Keratin 8+ glandular cells (red)(A) and α-SMA+ myoepithelial cells (red)(B). GFP+ cells in the developing SP (the area encircled by the dotted line) of glands co-express melanosomal proteins, TRP1 (C), TYR (D) and Pmel17/Silv (E) but not TuJ1 (F) or GFAP (G). TYR- immature GFP+ cells were also occasionally found in the SP (d, dotted arrow). Nuclei are counterstained with DAPI (blue). H–O, expression of GFP and various cell markers in the SP at P5 and 7wo. Down-regulation of the lineage markers Pax3, MITF or Dct was observed in GFP+ melanoblasts in the SP of adult mice (H-M). GFP+ melanoblasts were kept in an MCM2- quiescent state in the adult stage (I,K,O). P, Q, The number of GFP+TuJ1+ cells (arrowhead) in the dermis were profoundly reduced after sciatic denervation, while GFP+TuJ1- cells (arrows) were maintained in the SP. R,S, Immunostaining of the footpad sections of 7wo MITFce/+;Dct-H2B-GFPtg/+ (R) and MITFce/ce;Dct-H2B-GFPtg/+ (S) mice for GFP

and TuJ1 expression. GFP+TuJ1- melanocytes (arrows) were found in the SP of MITFce/+ but not in MITFce/ce mice. GFP+TuJ1+ neurons exist outside of the glands in both types of mice. T, The average number of GFP+TuJ1- melanoblasts per gland in a single footpad and per single hair follicles and the dermal GFP+TuJ1+ cells (per single footpad skin and per 1 mm width of dorsal skin) at 7 weeks in MITFce/+;Dct-H2B-GFP tg/+ and MITFce/ce;Dct-H2B-GFP tg/+ mice.

150x195mm (300 x 300 DPI)

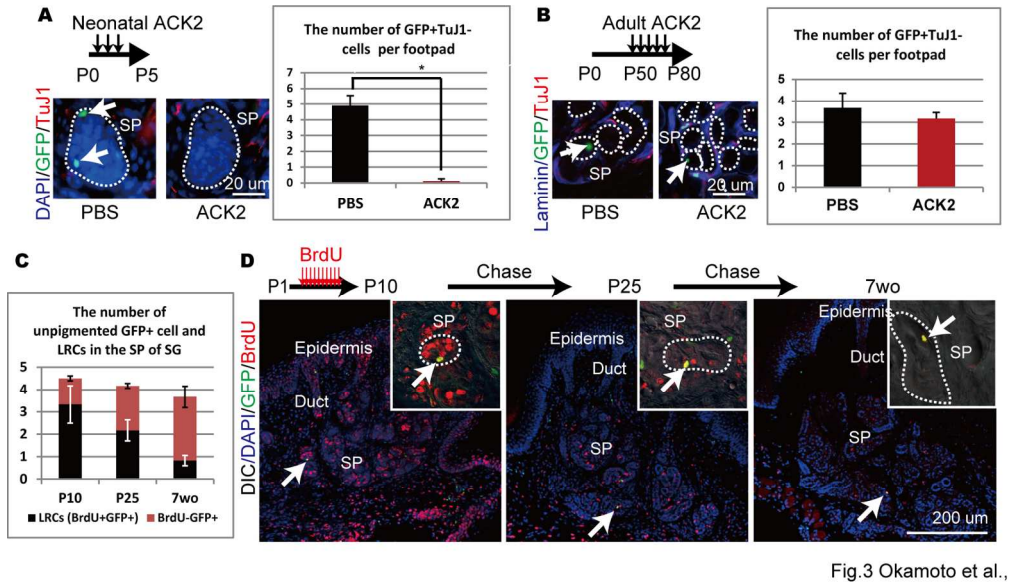

Fig.3 Okamoto et al.,

Figure 3. Dct-H2B-GFP+ cells are slow cycling, ACK2 resistant melanoblasts in adult skin. A-B, The differential ACK2 sensitivity of GFP+TuJ1- cells in sweat glands after ACK2 administration at the neonatal (A) or the adult stage (B). The number of GFP+TuJ1- cells in the SP is shown. A, While GFP+TuJ1- cells are found in the SP of control mice (green; arrows), almost no GFP+TuJ1- cells remain in the SP of neonatal ACK2-treated mice. B, GFP+TuJ1- cells remain in the SP of adult ACK2-treated mice. Error bars represent s.d. of 3 independent experiments. *, statistical significance at the level of $P < 0.01$. C-D, Pulse-chase experiments with BrdU in Dct-H2B-GFP tg mice. The total number of GFP+TuJ1- cells in the SP did not significantly change from post-neonatal (P10) to adult stage (7wo) (C). After continuous BrdU injection (P1-P10), almost all cells in the acral skin of Dct-H2B-GFP tg mice were labeled with BrdU at P10 (D; arrows (SP)). At P25 and 7wo, GFP+ melanoblasts were found exclusively in the SP of sweat glands with significant retention of BrdU (D). The label is still retained in some GFP+ melanoblasts at 7wo (D; arrows and C). The insets show magnified images of GFP expressing cells.

147x85mm (300 x 300 DPI)

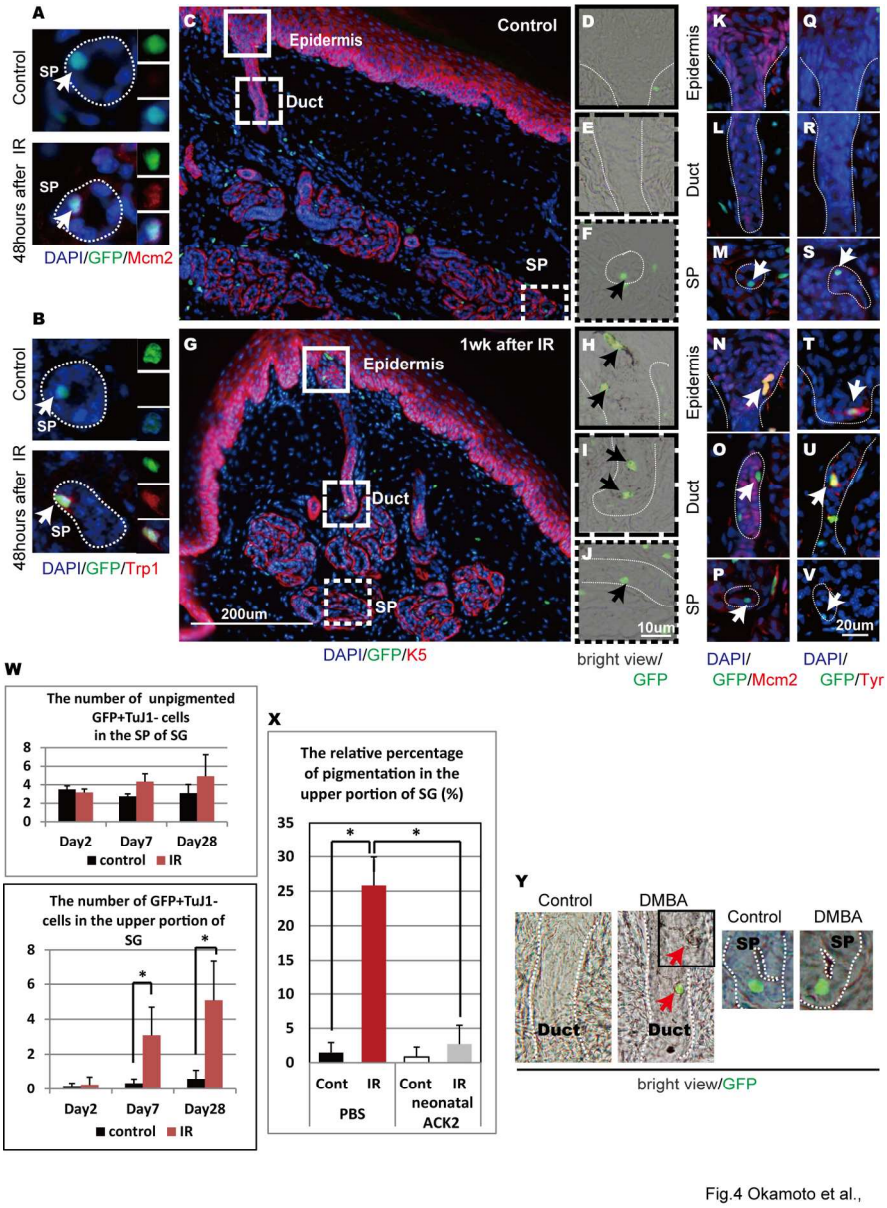

Fig.4 Okamoto et al.,

Figure 4. Melanoblasts in the SP of sweat glands maintain themselves and provide proliferating and differentiating melanocytes to the epidermis in response to IR or oncogenic stress.

A-T Behavior of GFP+ cells in sweat glands after 5 Gy IR. Immunostaining for keratin 5 (K5) was performed on footpad skin sections in Dct-H2B-GFP tg mice to chase GFP+ cells (green) located within the glands after IR. While no GFP+ cells exist in the duct or the epidermis in control mice (A-D), GFP+ cells (arrows) exist in the duct and the epidermis after IR at 1 week (1wk) (E-H). Bright view images merged with GFP images are shown for the epidermis (solid-line square) (B, F), the sweat duct (marked by the long-dashed line square) (C, G) and SP (the short-dashed line square) (D, H) on the right side of the large panel. Melanogenesis can be observed only in the duct or in the epidermis (F, G). I-N and O-T, MCM2 and TYR immunostaining images are shown respectively on the right side of the figure. Most GFP+ cells (arrows) at the SP are MCM2- (K,N), while IR-induced ductal or epidermal GFP+ melanocytes (arrows) are MCM2+ (red) (M,L) and TYR+ (red) (R,S). U,V, Transient cell cycle entry and commitment of GFP+ cells in the SP. At around 48 hr after IR, expression of MCM2 and TRP1 was found transiently in some GFP+ cells located within the SP (arrow). W,

The number of GFP+ cells located in the SP remained stable after IR(graph in the upper column), while the number of GFP+ cells located within the duct of glands after IR was significantly increased (graph in the lower column). *, statistical significance at the level of P < 0.05. X, IR-induced pigmentation of the upper portions of glands after IR was dramatically impaired when mice were pretreated with ACK2 at the neonatal stage (Z). Error bars represent s.d. of 3 independent experiments. *, statistical significance at the level of P < 0.01. Nuclei are counterstained with DAPI (blue). Y, Pigmented GFP+ cells (red arrow) were found in the duct at 4 weeks after DMBA, while GFP+ cells in the SP were kept in an unpigmented state.

147x200mm (300 x 300 DPI)

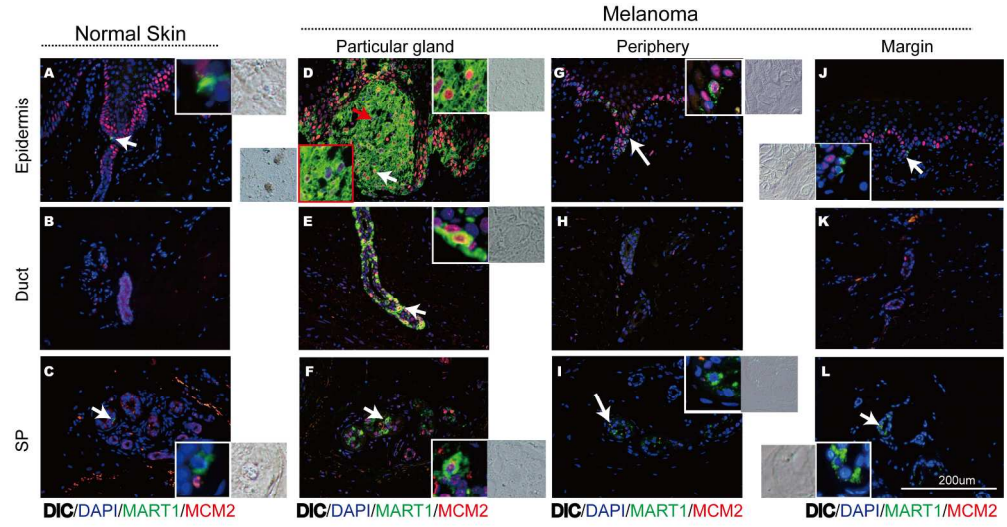

M

	Sample	Age/Sex	Size	Thickness	Epidermis: Furrow Area (CPL)	Epidermis: Ridge Area (CPI)	Duct: particular gland	Duct: others	Secretory Portion: particular gland	Secretory Portion: others
Normal Skin	A	32/F	-	-	-	+	-		+	
	B	62/F	-	-	-	+	-		-	
	C	51/F	-	-	-	+	-		+	
Melanoma	D	78/F	23x23	in situ	+	++	-	-	+	+
	E	56/F	20x12	in situ	+	++	+	-	+	+
	F	79/F	15x15	in situ	+++	+++	++	-	+	+
	G	95/M	70x30	0.9	+	++	++	-	+	+
	H	93/F	33x30	3.2	+	+++	+	-	+	+
			(mm)	(mm)						

CPL, crista profunda limitans; CPI,crista profunda intermidia
-, no MART1+ cell in 10 sections; +, 1-3 MART1+ cells in 10 sections; ++, 3-10 MART1+ cells in 10 sections; +++, more than 10 MART1+ cells in 10 sections; red, MCM2+MART1+ cells.

Fig.5 Okamoto et al.,

Figure 5. Identification of melanoblasts in the SP of human volar sweat glands as an expandable source of early acral melanoma.

A-L, Localization of melanocyte/melanoma cells and their cell cycle status in human volar sweat glands. Human normal volar skin (A-C) and early melanoma skin (D-L) were immunostained for the lineage markers, MART1 (shown in green) and MCM2 (in red). A small number of MART1+MCM2- cells is found in the epidermis close to the sweat duct within the ridge area of the skin (A) and the SP (C) but not within the duct (B). D, A nest of MART1+MCM2+ unpigmented melanoma cells (white arrows) and MART1+MCM2low pigmented melanoma cells (red arrows) was found in the epidermis of the ridge area of the lesional skin of melanoma in situ. MART1+ cells are aligned contiguously throughout the duct (arrow; E) and SP (arrow; F) area of a particular sweat gland within the center of the lesion. At the periphery of the lesion, MART1+MCM2+ cells were found in the epidermis (arrow; G) but not in sweat glands (arrow; I). At the intact margin, there are MART1+MCM2- melanoblasts but no MART1+MCM2+ cells in the epidermis (J). The SP of an identical gland contains a MART1+MCM2- melanoblast (L). Note that MART1+ cells were found in the duct of particular glands at the lesion but not in the surrounding glands at the margin of the lesion (H and K). Magnified images of MART1+ cells are shown in the insets. Nuclei are counterstained with DAPI. M, Table showing the distribution and proliferative status of MART1+ cells in human acral skin samples. In normal control skin samples, a small number of MART1+ cells were found in the SP and most of them are MCM2-, while those in early melanoma lesions are MCM2+ and MART1+MCM2+ proliferative cells were found in the sweat duct and SP of particular glands.

206x202mm (300 x 300 DPI)

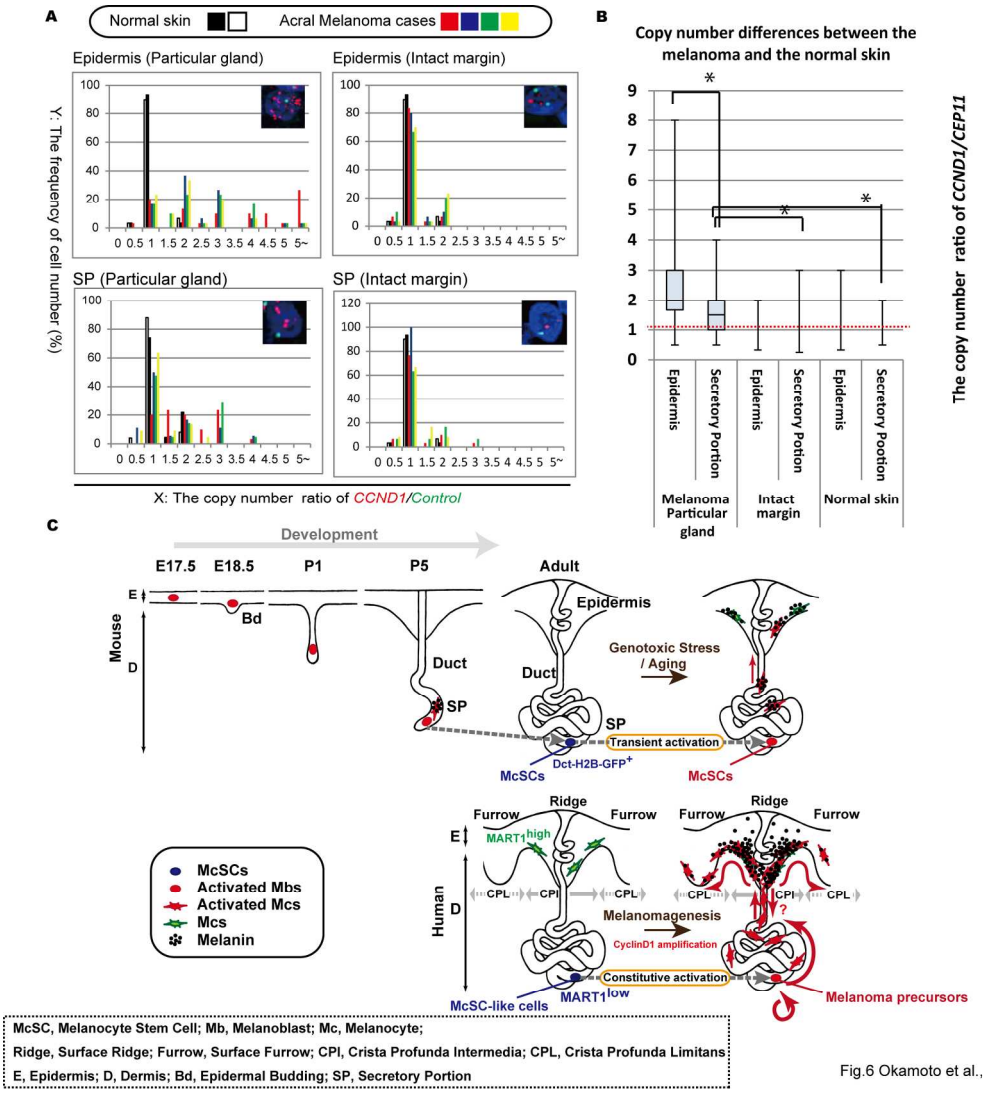

Fig.6 Okamoto et al.,

CCND1 gene amplification in the SP within a melanoma lesion and a schematic for McSC-like cell development, maintenance and melanomagenesis.

A. Histograms showing the distribution of copy number variation of 11q13 CCND1 genomic regions in the tumor center of early acral melanomas. Colored bars (red, blue, green, and yellow) show individual samples derived from acral melanoma cases, while colored bars (black and white) show control normal samples. The Cep11 centromeric region was used to normalize FISH signals between cells at different cell cycle stages. B. Box plot showing the copy number differences between the epidermis and SP from melanoma and normal skin. Copy number amplification of the CCND1 gene is found in the SP of sweat glands within the lesion but not in the normal skin, is significantly lower than that seen in the epidermis. *, statistical significance at the level of $P < 0.05$. C. The fate and behavior of melanocyte lineage cells in sweat glands are summarized and combined with a hypothetical schematic for melanoma initiation from McSC-like cells. Proliferating melanoblasts (red) which colonized the SP of the sweat glands enter a quiescent (Go) state just after development and become McSC-like cells maintained in a dormant state (blue). These McSC-like cells are activated transiently by extrinsic or intrinsic stresses such as genotoxic stress and during the normal ageing process. Conversely, the corresponding population in the SP maintains its cycling activity to renew the population and to generate their amplifying and differentiating progenies to transfer to the epidermis through the ducts which connect the SP and the epidermis with further acquisition of genetic alterations.

Thus McSC-like cells are most likely to serve as an origin of melanoma or melanoma-initiating cells.
182x197mm (300 x 300 DPI)

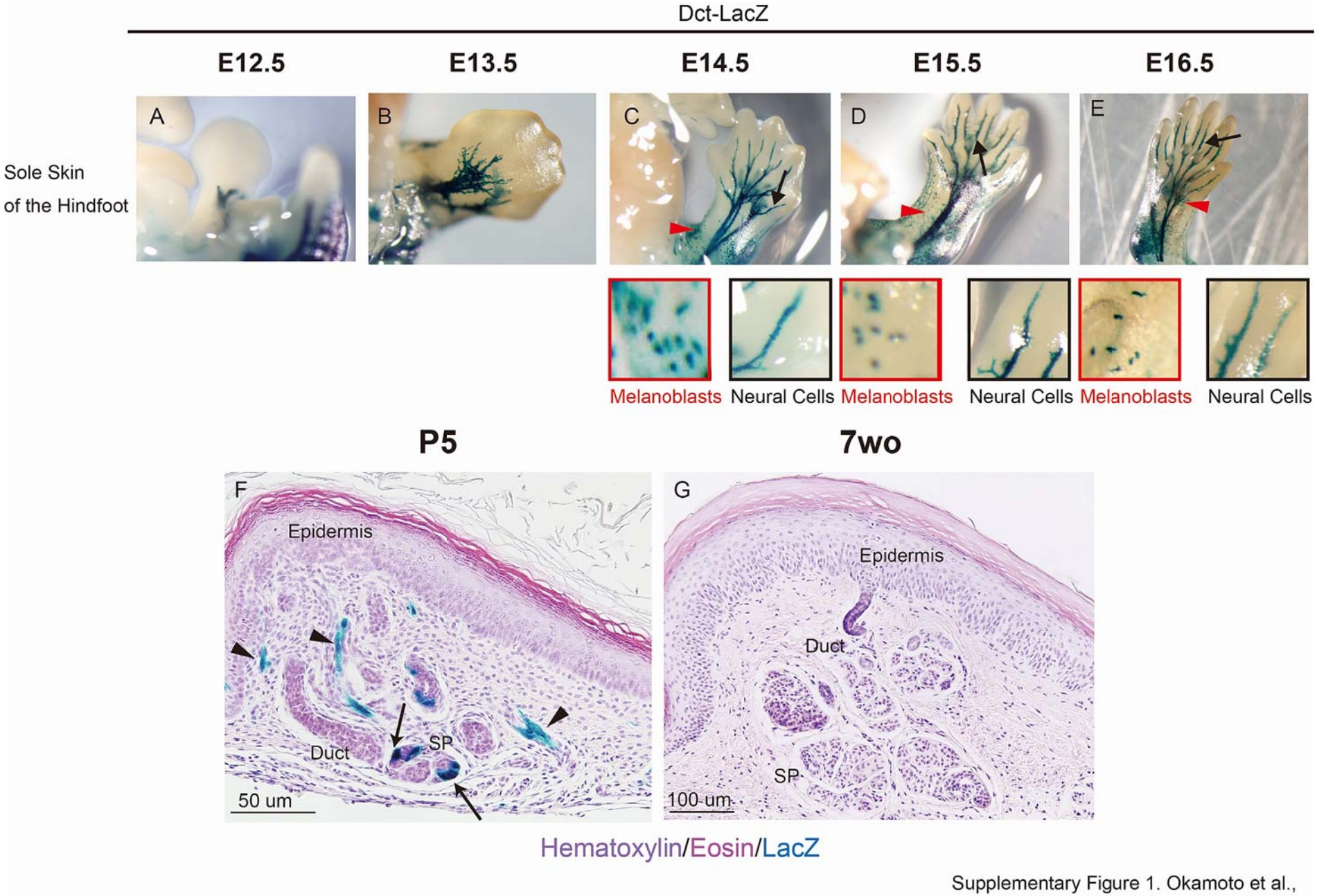

Supplementary Figure 1. Okamoto et al.,

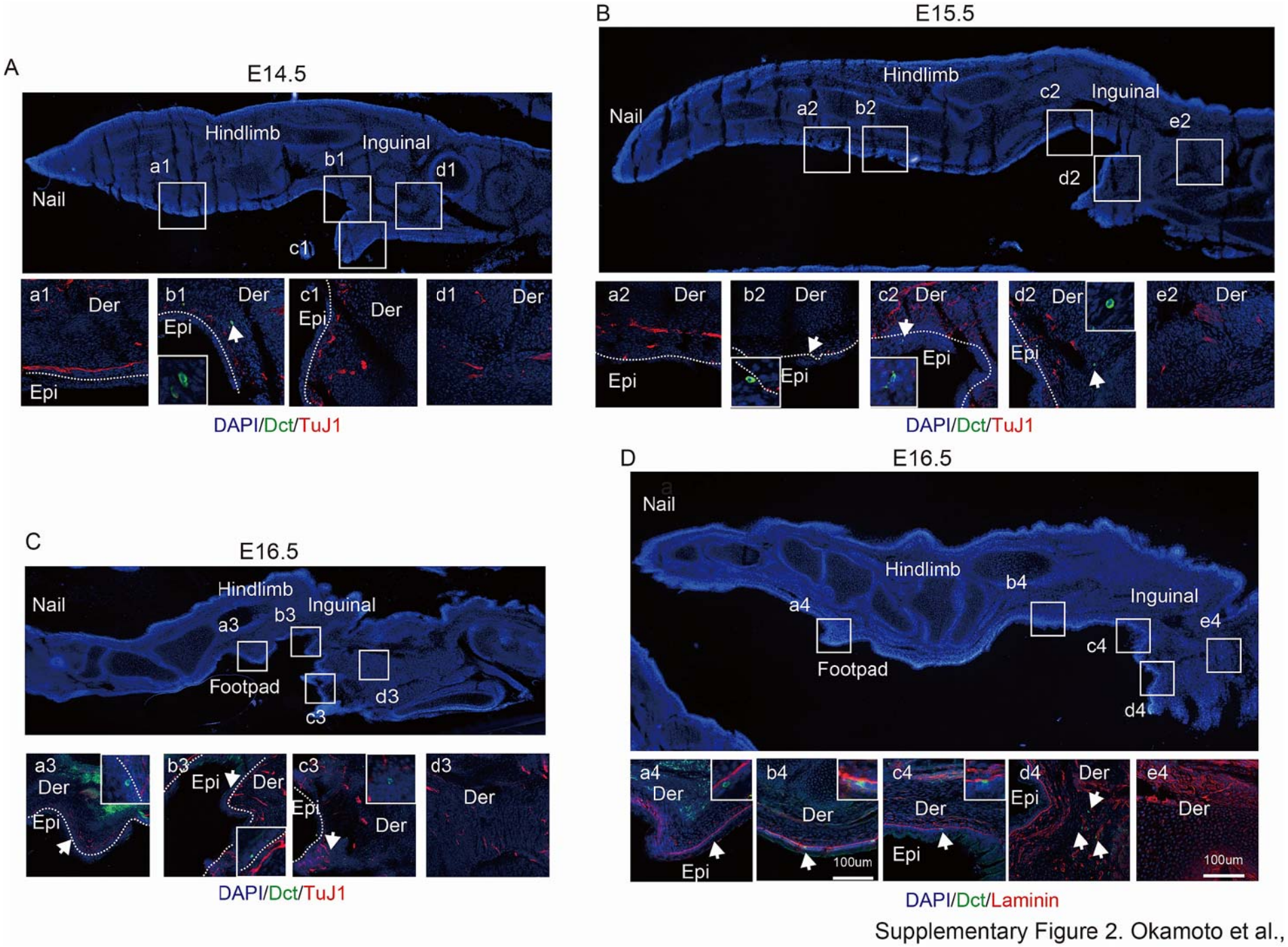

Supplementary Figure 2. Okamoto et al.,

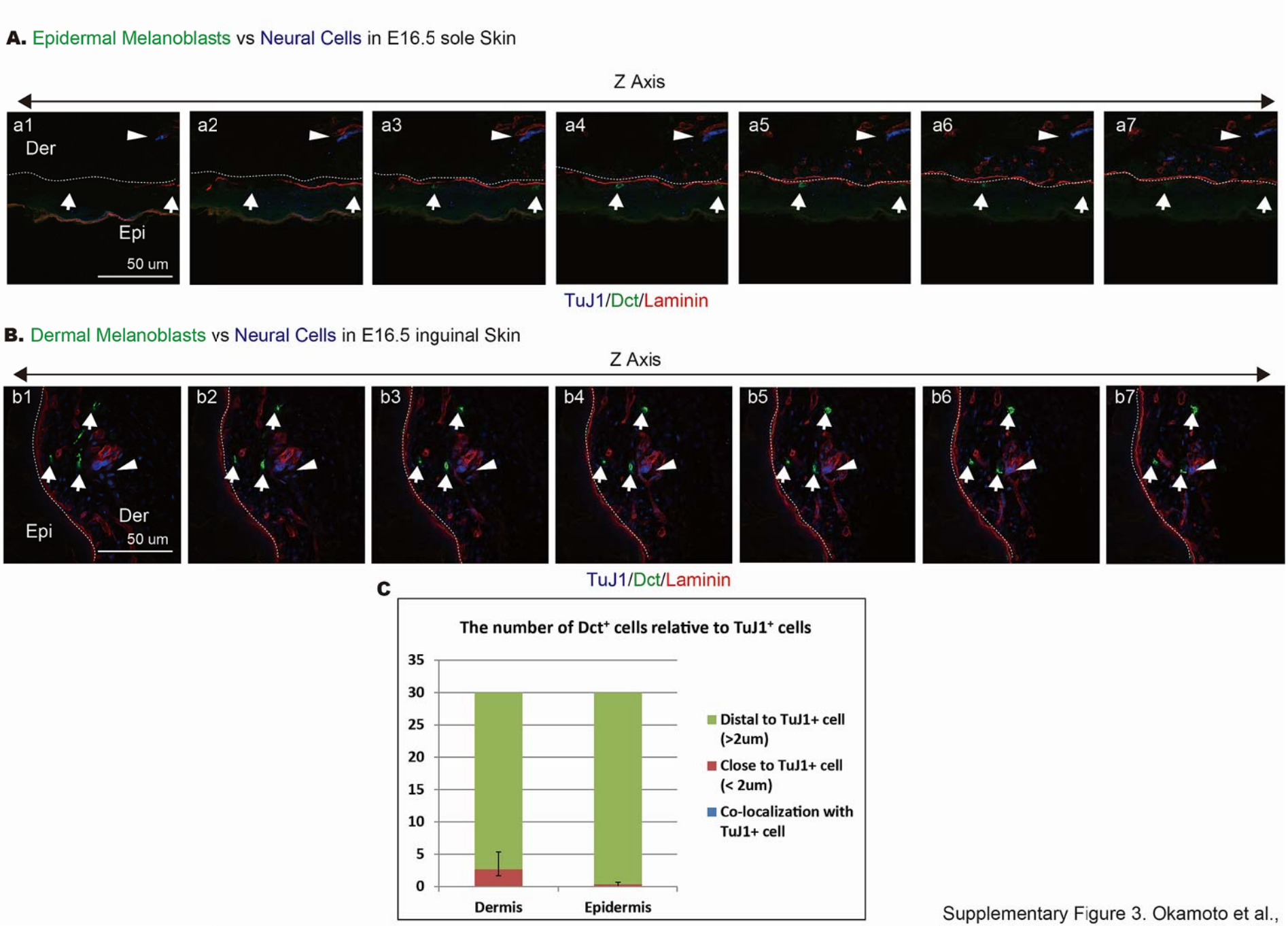

Supplementary Figure 3. Okamoto et al.,

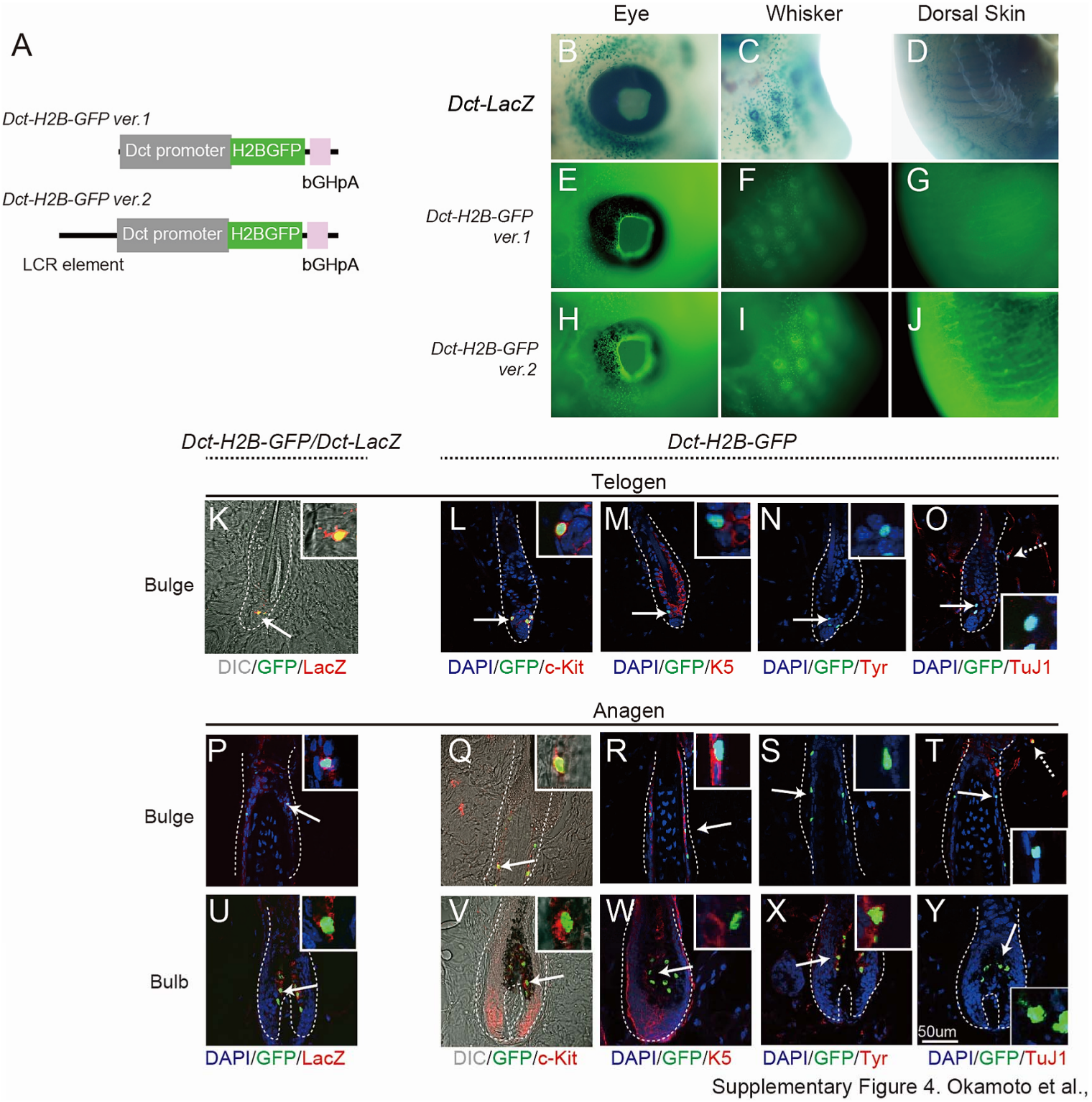

Supplementary Figure 4. Okamoto et al.,

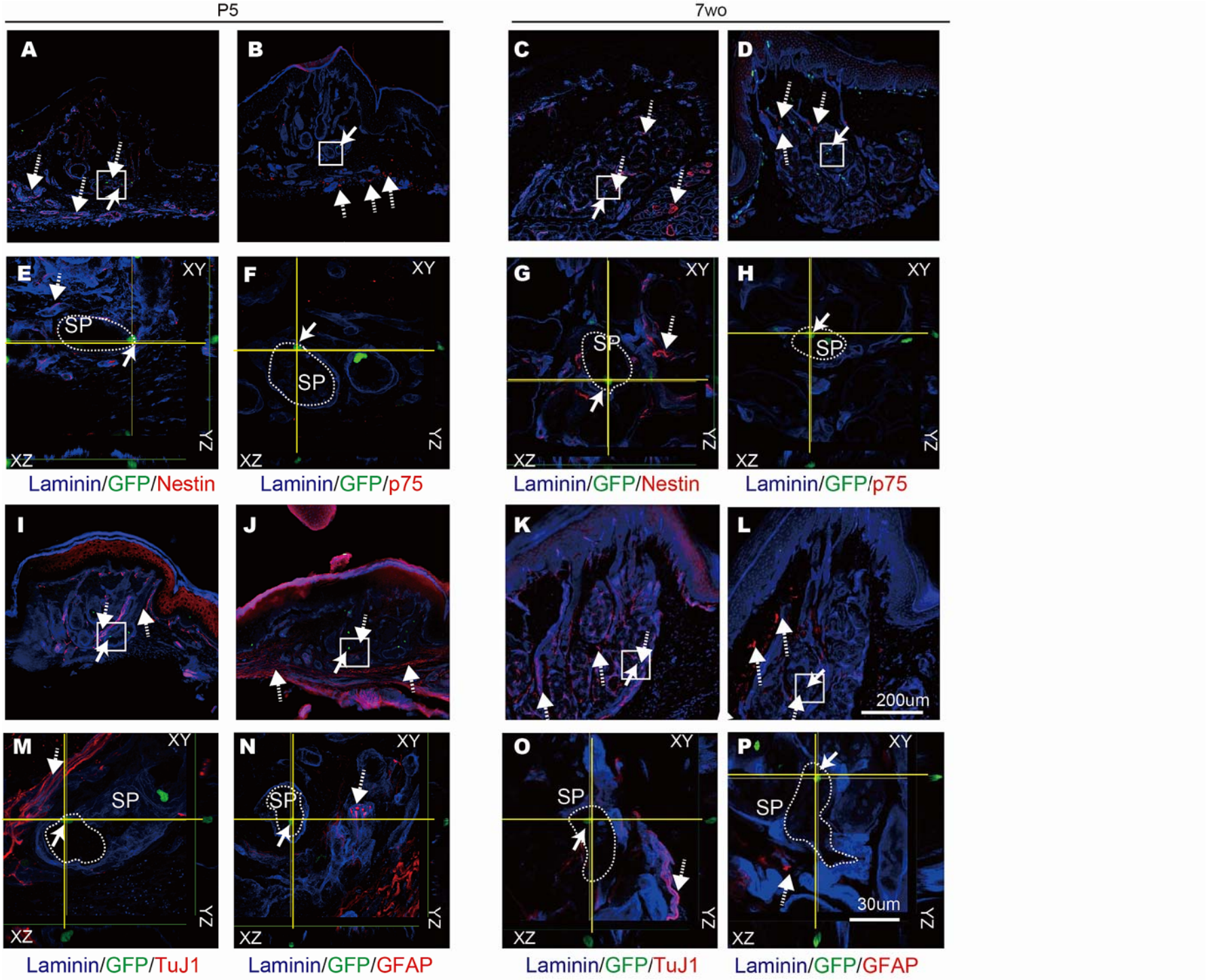

Supplementary Figure 5. Okamoto et al.,

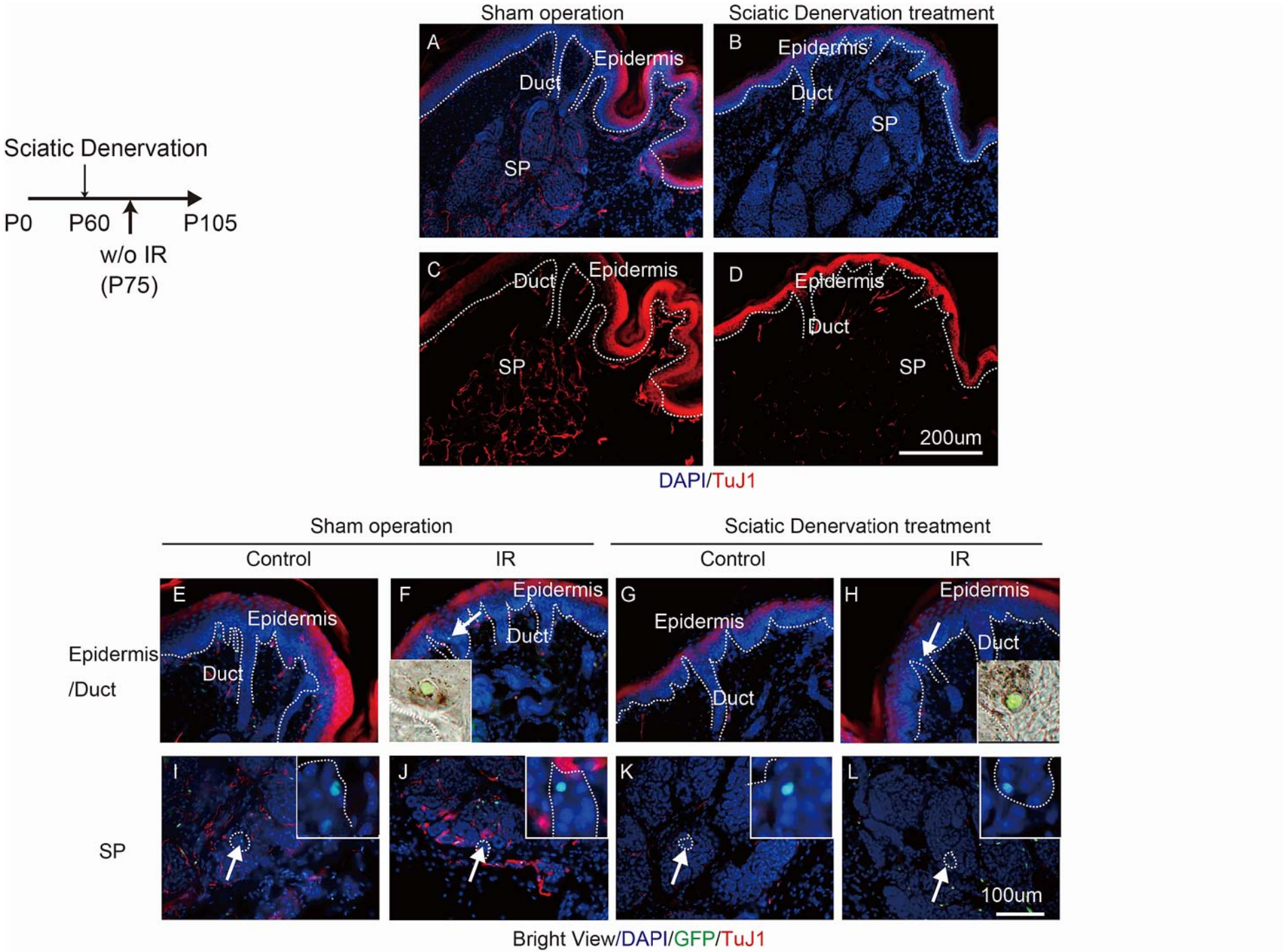

Supplementary Figure 6. Okamoto et al.,

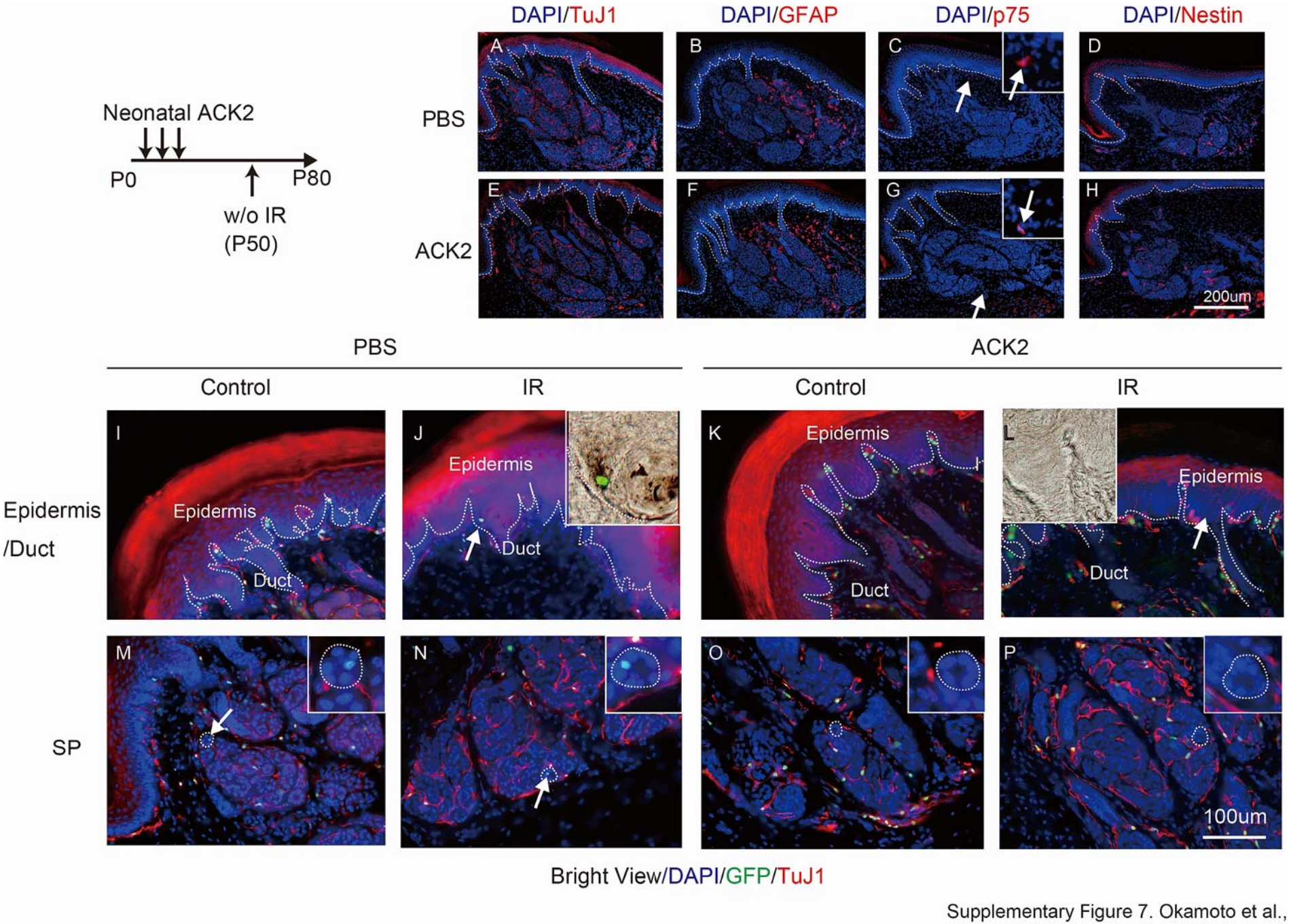

Supplementary Figure 7. Okamoto et al.,

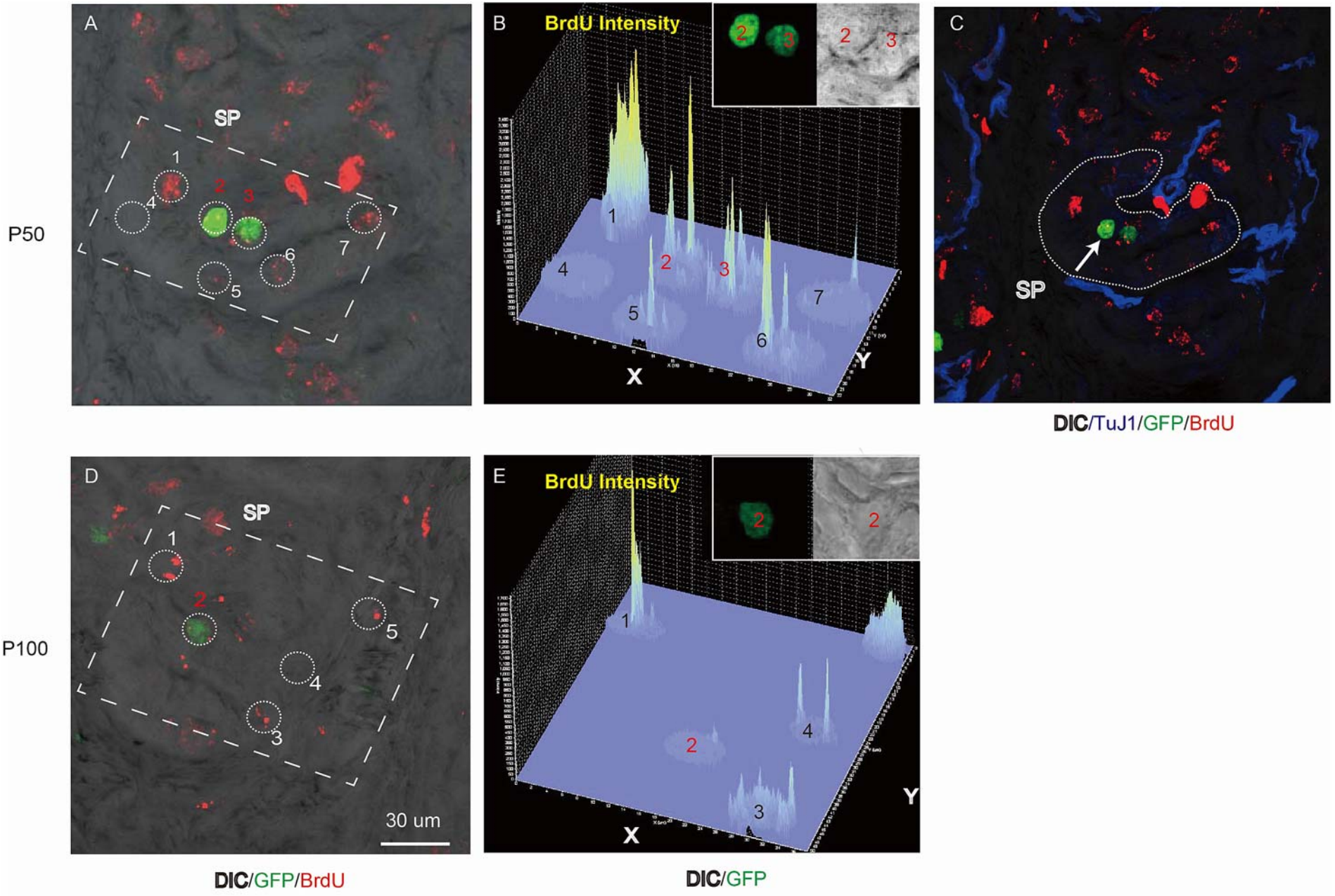

Supplementary Figure 8. Okamoto et al.,

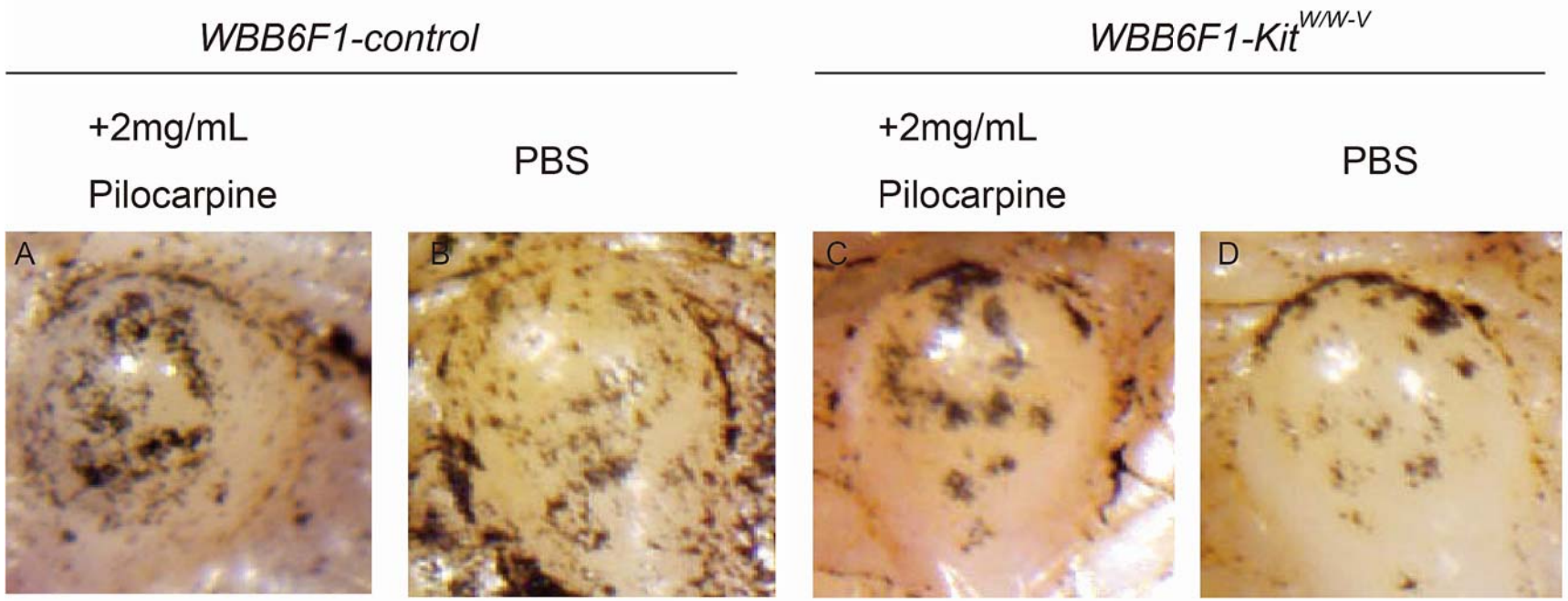

Supplementary Figure 9. Okamoto et al.,

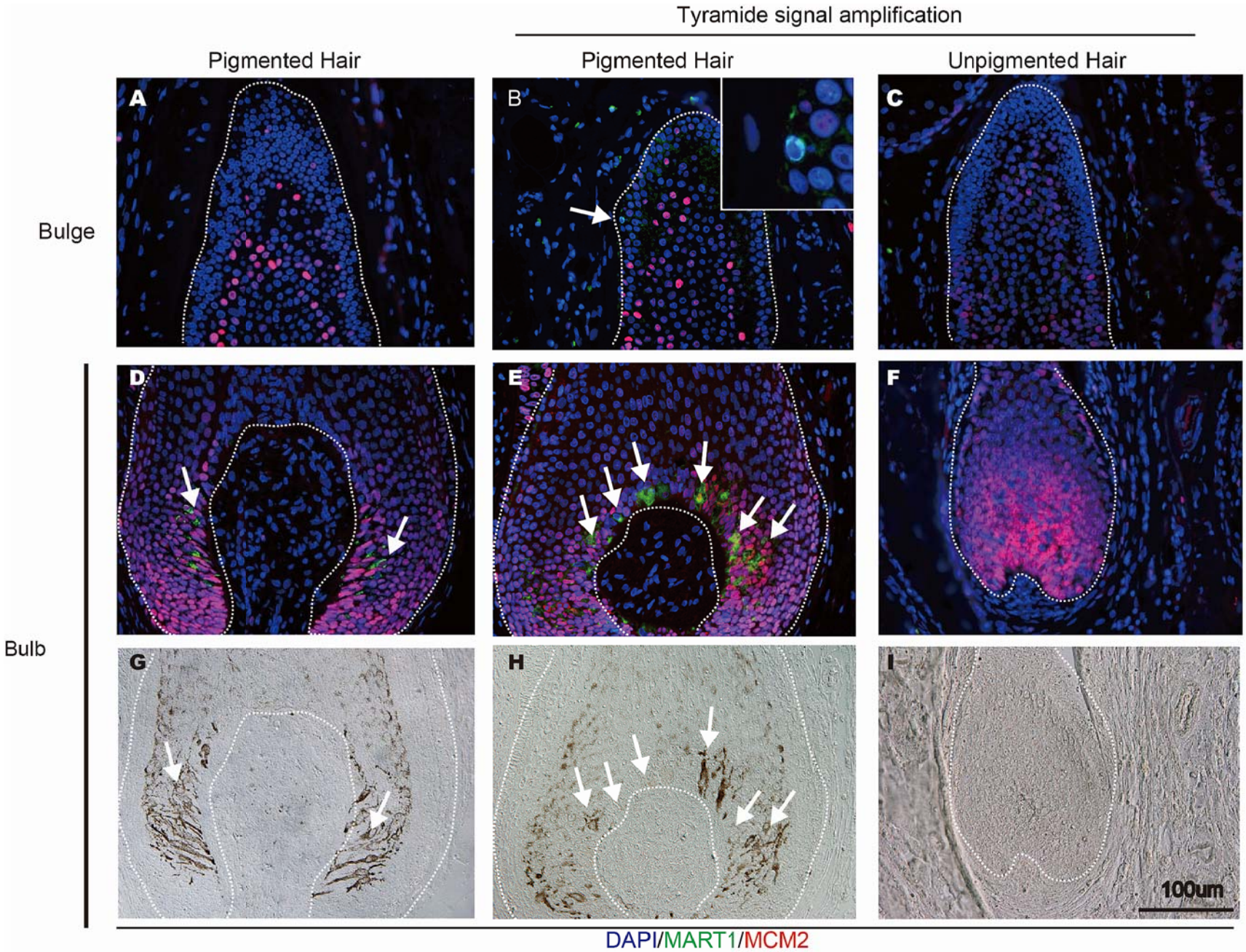

Supplementary Figure 10. Okamoto et al.,

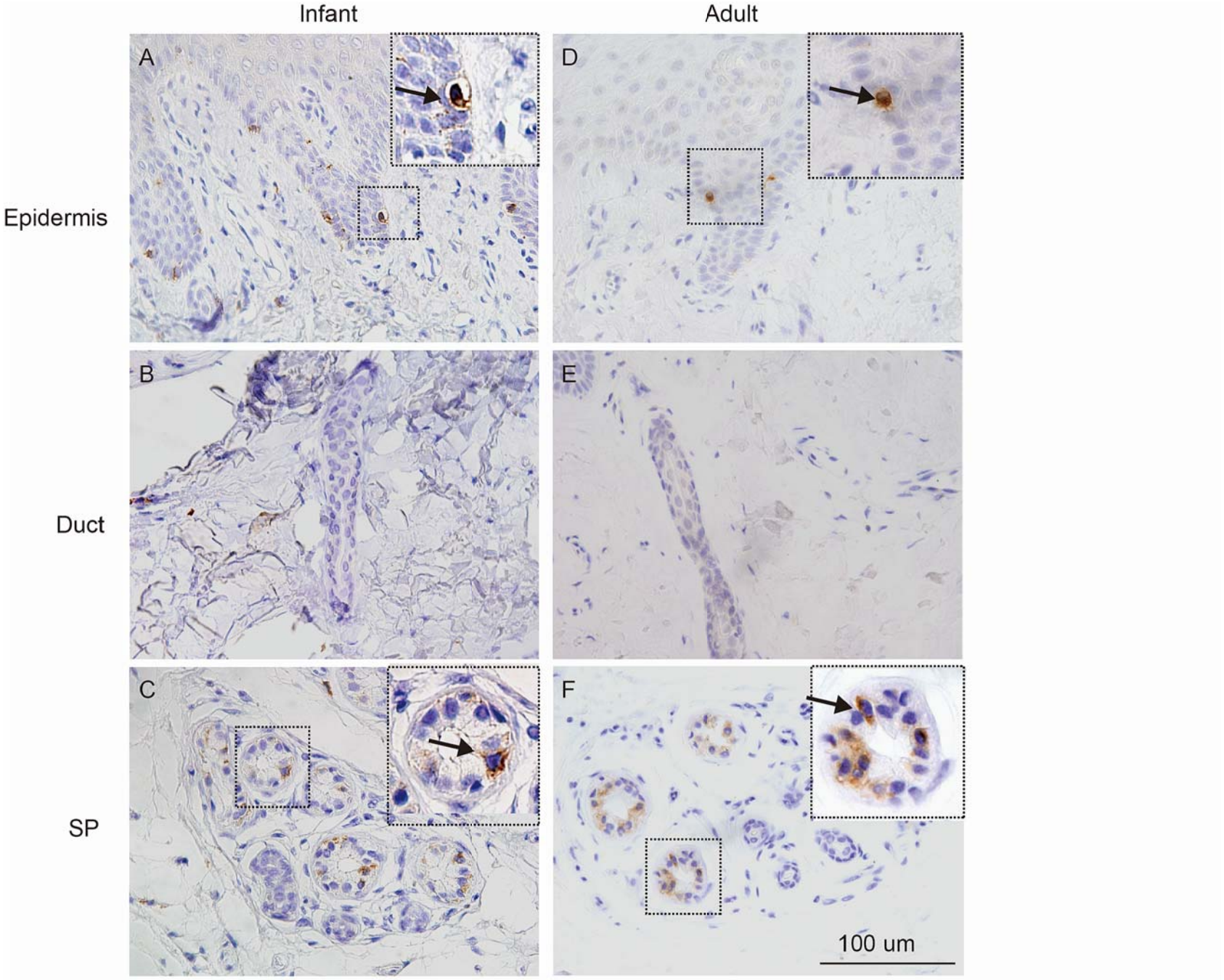

Supplementary Figure 11. Okamoto et al.,

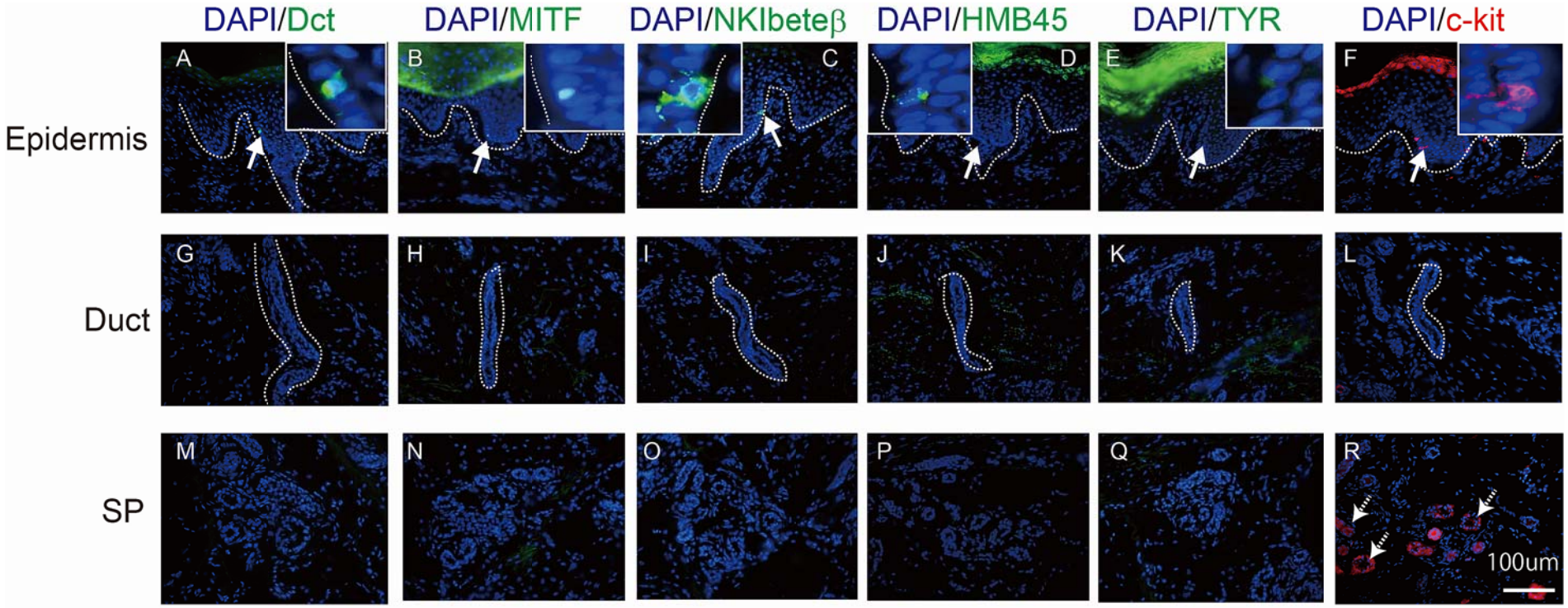

Supplementary Figure 12. Okamoto et al.,

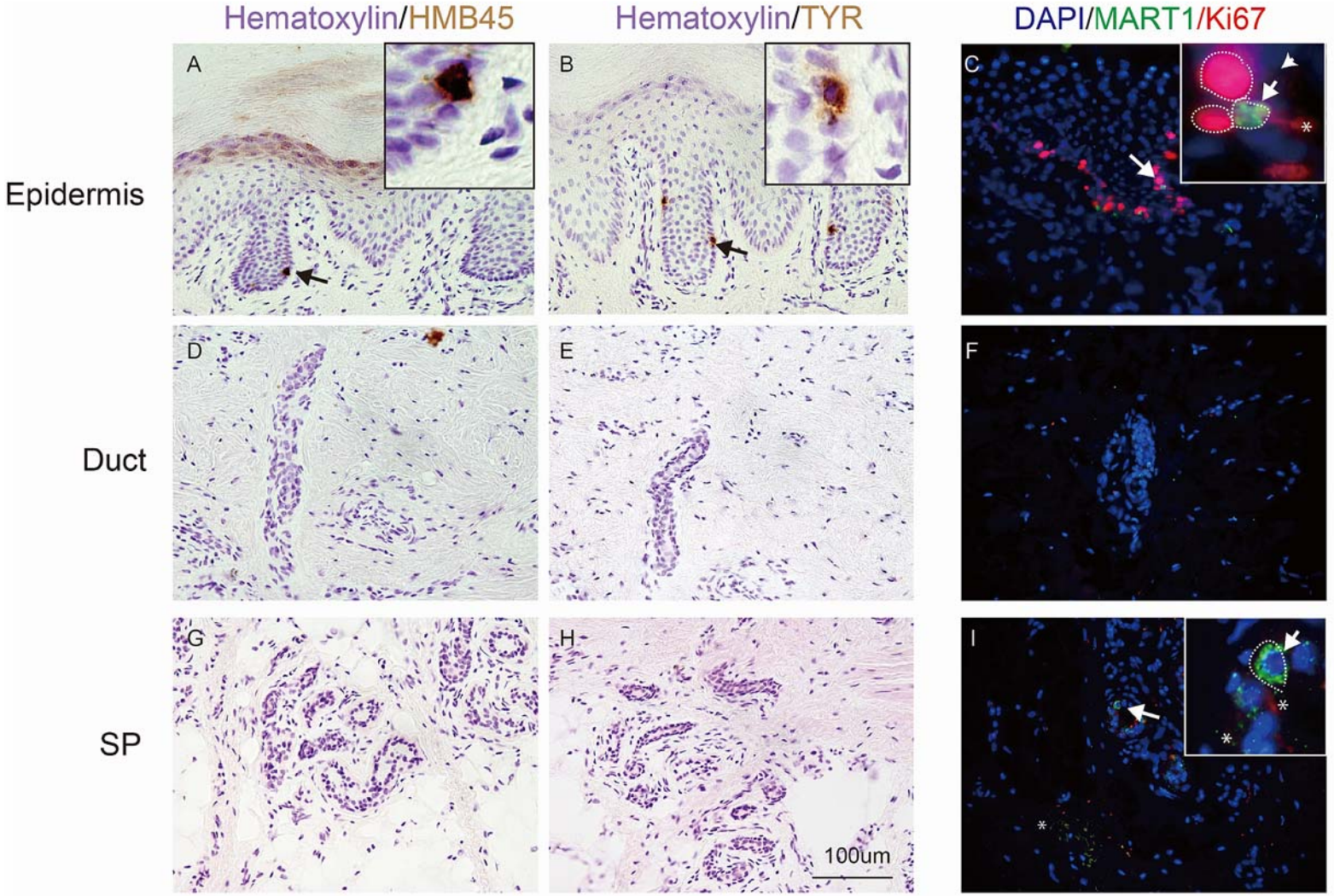

Supplementary Figure 13. Okamoto et al.,

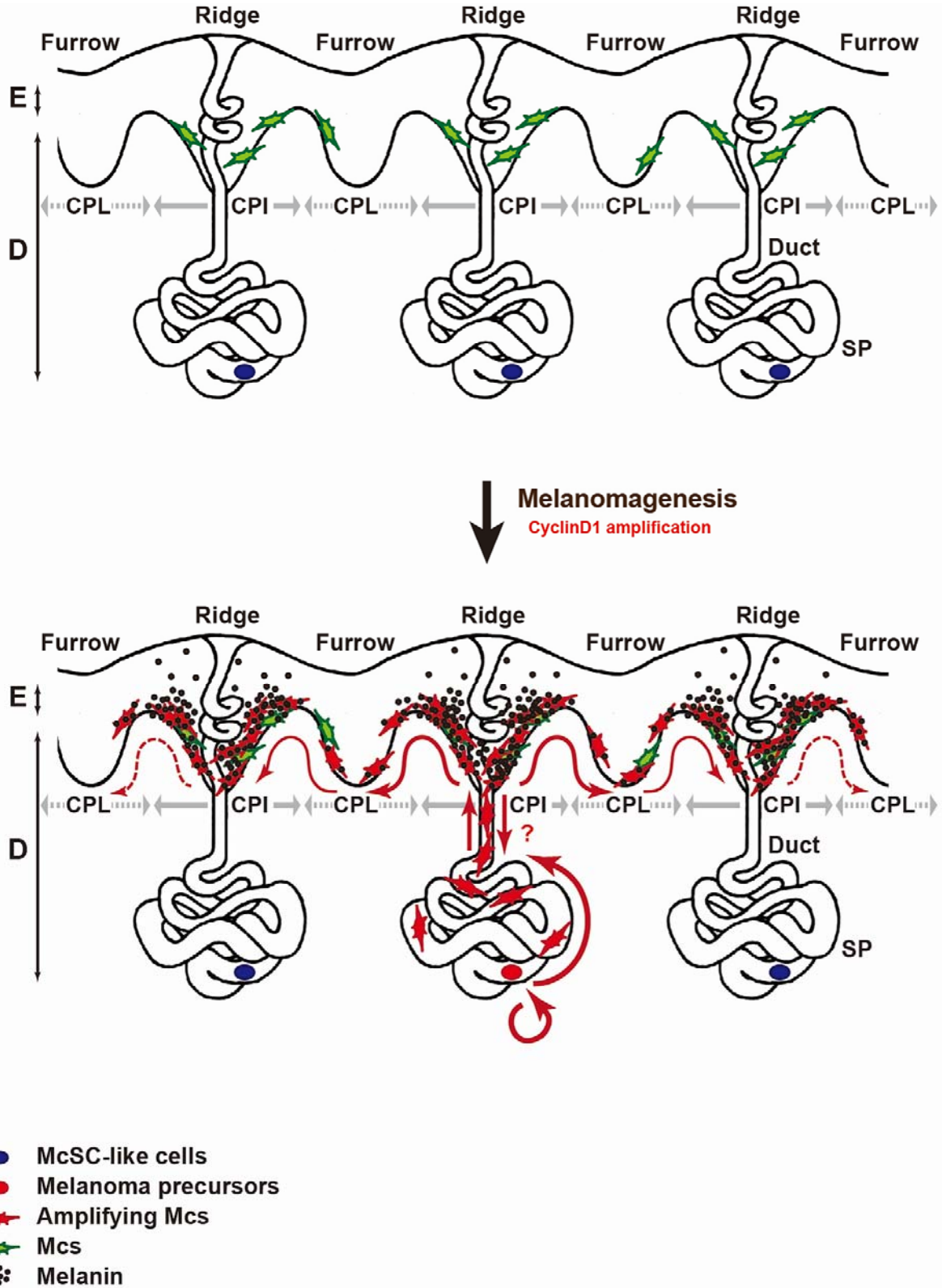

McSC, Melanocyte Stem Cell; Mc, Melanocyte;

Ridge, Surface Ridge; Furrow, Surface Furrow; CPI, Crista Profunda Intermedia; CPL, Crista Profunda Limitans

E, Epidermis; D, Dermis;

Supplementary Figure 14. Okamoto et al.,

Supplementary documents

Supplementary Figure Legends

Supplementary Figure 1

Distribution of developing melanoblasts and peripheral neurons in the distal hindlimb of mouse embryos.

A-E, Shown are the whole mount LacZ staining of the distal hindlimb of *Dct-LacZ* tg mice. Not only migrating melanoblasts (red arrowheads) but also developing peripheral neurons (black arrows) are visualized (**A-E**). $LacZ^+$ melanoblasts (Mbs), which have dispersed throughout the dorsal trunk by embryonic day 13.5 (E13.5), appear around the inguinal regions, the junction between the trunk and the limbs at E14.5 (**C**), and are subsequently found more distally throughout the legs at E15.5 (**D**). At E16.5, $LacZ^+$ melanoblasts are found in hindfoot (**E**). Note that $LacZ^+$ melanoblasts do not appear at the distal ends of developing peripheral nerves. Instead they are distributed at the leading edge of the migrating melanoblasts proximally to the trunk. The red-lined and black-lined inset boxes show magnified images of the melanoblasts and neural cells, respectively. **F**, **G**, HE staining of LacZ-stained skin sections of the footpad (**F**; 5-day-old (P5) and **G**; 7-week–old (7wo)). $LacZ^+$ melanocytic cells are found at the tip of the sweat duct and in the SP of glands at P5 (arrows), while no $LacZ^+$ cells are detectable at 7-weeks-old (7wo). Arrowheads indicate $LacZ^+$ neural cells in the dermis.

Supplementary Figure 2

Migration of developing melanoblasts into the epidermis for their eventual colonization of the footpad epidermis in mice.

A-D, Distribution of Dct^+ melanoblasts in developing hindlimb skin was visualized by immunostaining of the Dct protein at different developmental stages (**A**: E14.5; **B**: E15.5; **C-D**: E16.5). In the sole skin, migrating Dct^+ melanoblasts (green; arrows) are detectable in the dermis around inguinal regions and in the epidermis throughout hindlimb and budding sweat gland at E14.5-E15.5 (**A-a1; B-b2**). Note that Dct^+ cells do not express the neural marker TuJ1 (red) in the epidermis or dermis of the sole skin, indicating that Dct^+ cells which are migrating into the epidermis and then into the budding sweat glands can be distinguished from non-melanocytic cells without showing any significant association with neurons. (**A**). Basement membranes at the dermal-epidermal junction were labeled with Laminin (red) (**D:a4-e4**) to distinguish the epidermis and dermis. Nuclei were counterstained with DAPI (blue). Magnified images for each

stage (a1-e4) were taken by confocal microscopy.

Supplementary Figure 3

Dct-expressing melanoblasts in sole skin do not coexpress a neural lineage marker TuJ1.

A, B, Shown are images of the sole or inguinal skin of the developing hindlimb (E16.5) and each Z- axis figures. Epidermal Dct+ melanoblasts (Green; white arrows) were often found to be associated with the basement membrane (Red; dotted line), while TuJ1+ cells (Blue; red arrowheads) were found exclusively in the dermis (**A: a1-a7**). Most dermal Dct+ melanoblasts (Green; white arrows) are found away from the TuJ1+ neural cells (Blue; red arrowheads) (**B: b1-b7**). **C**, The graph shows the rate of association or co-localization between Dct and TuJ1 cells. Although a minor population of Dct+ cells are located within 2 μm distance to neural cells in the dermis around the inguinal region (**B**), Dct+TuJ1+ double-positive cells were never found anywhere in the sole skin by 3D reconstituted confocal microscopy analysis. A three-dimensional image was reconstructed from at least 40 serial 0.4 μm confocal sections and representative images are shown as sequential images.

Supplementary Figure 4'

Characterization of *Dct-H2B-GFP* transgenic (tg) mice.

A, Structure of the *Dct-H2B-GFP* transgene (ver.1 and ver.2): *H2B-GFP* reporter under the melanocyte-specific *Dct* promoter and LCR elements from the *Tyr* gene. **B-J**, Appearance of eyes (**B, E, and H**), whiskers (**C, F, and I**) and dorsal skin (**D, G, and J**) of *Dct-LacZ*, *Dct-H2B-GFP ver.1* and *Dct-H2B-GFP ver.2* tg mice at embryonic day 14.5. **K, P, U,** Immunofluorescent staining of adult *Dct-H2B-GFP; Dct-LacZ* compound tg mice revealed that GFP signals colocalized with that of LacZ (red) in GFP^+ cells (green; arrows) both in the bulge and in the hair follicle bulb. **L-O**, **Q-T**, **V-Y,** Immunofluorescent staining of the dorsal skin of *Dct-H2B-GFP* tg mice showed that Kit expression (red) colocalizes with the GFP signal (green) both in the bulge and in the bulb through the hair cycle (**L**, **Q,** and **V**). The GFP^+ cells do not express the basal keratinocyte marker keratin 5 (**M**, **R,** and **W**). The GFP^+ cells in the bulb expressed Tyr (tyrosinase) (red) at anagen but those in the bulge did not (**N**, **S,** and **X**). A subset of GFP^+ cells located in the dermis (**O**, **T**, dotted arrows) co-expressed the neural marker TuJ1 (red), but those in the hair follicle (**O**, **T**, arrows) failed to express TuJ1. The insets show magnified images of GFP-expressing cells.

Supplementary Figure 5

GFP$^+$ cells in the sweat glands of *Dct-H2B-GFP* tg mice are distinct from Nestin$^+$ neural progenitors, p75$^+$ neural crest progenitors, TuJ1$^+$ neurons, and GFAP$^+$ Schwann cells.

Immunofluorescent staining of the footpad skin of *Dct-H2B-GFP* tg mice at postnatal day 5 (P5) and 7 weeks old (wo). The images show that GFP$^+$ melanoblasts (arrows) are located inside the SP of sweat glands at both P5 and 7wo. GFP$^+$ melanoblasts (arrows) in the SP area of gland are distinct from the cells positive for Nestin (a neural progenitor marker) (**A**, **C**, **E**, **G**: red: dotted arrow), p75 (a neural crest progenitor marker) (**B**, **D**, **F**, **H**: red: dotted arrow), TuJ1 (a neuronal marker)(**I**, **K**, **M**, **O**: red: dotted arrow) or GFAP (a Schwann cell marker) (**J**, **L**, **N**, **P**: red: dotted arrow). The basement membrane is shown by Laminin distribution (blue). Nuclei are counterstained with DAPI (blue). Magnified views of the white-lined inset boxes are shown below. Three-dimensional images were reconstructed from at least 40 serial 0.4 μm confocal sections and are shown besides individual images (**E-H, M-P**).

Supplementary Figure 6

GFP$^+$ melanoblasts in the SP of sweat glands of denervated footpads provide their pigmented progenies to the epidermis after IR.

Immunofluorescent staining of footpad skin of *Dct-H2B-GFP* tg mice after sciatic nerve denervation with or without (w/o) 5Gy IR. **A-D,** The number of TuJ1$^+$ neural cells (red) in the dermis was profoundly reduced after sciatic denervation. Nuclei are counterstained with DAPI (blue). **E-L,** Distribution of GFP$^+$ cells in sweat glands after sciatic denervation (on P60) and subsequent IR treatment (on P75). While no GFP$^+$ cells were found in the epidermis in control mice (**E** and **G**), pigmented GFP$^+$ cells (green; arrows) were found in the epidermis after IR in both control and denervated footpads. Bright view images merged with GFP images of epidermal melanocytes found in irradiated mice are shown (**F** and **H**). GFP$^+$ melanoblasts were found in the SP of glands in both control and denervated mice after IR (**I** – **L**). The insets show magnified images of GFP expressing cells. Nuclei were counterstained with DAPI (blue).

Supplementary Figure 7

Depletion of developing McSCs in acral skin eradicates the IR-induced appearance of melanocytes in sweat glands and in the epidermis.

Dct-H2B-GFP tg mice were treated with ACK2 at the neonatal stage and were then irradiated with or without (w/o) 5 Gy IR at P50. **A-H**, Distribution of cells expressing neuronal/glial lineage-related markers (TuJ1, GFAP, p75 and Nestin) in the footpads showed no difference with or without ACK2 treatment. **I-P**, GFP$^+$ cells were depleted from the SP of sweat glands after ACK2 treatment (**O**). IR-induced appearance of differentiated melanocytes in the ducts and the epidermis were not found in ACK2-treated mice (**L**). Bright view images merged with GFP

images are shown in the insets. Nuclei were counterstained with DAPI (blue).

Supplementary Figure 8

Slow-cycling GFP$^+$ melanoblasts exist in the SP area of sweat glands in adult acral skin under physiological conditions.

A-E, BrdU pulse-chase experiments was performed similarly to Figure 2U-W**.** Representative images of BrdU retention in GFP$^+$ cells are shown. The abundant BrdU retention in the GFP$^+$ cells was observed in GFP^{high} cell clone (#2 and #3) at P50 (**A, B**), while diminished levels of BrdU retention was found in GFP$^+$ cells at P100 (**D, E**) in the SP of glands. BrdU$^+$GFP$^+$ cells in the SP area are distinct from TuJ1$^+$ neurons (**C**). Measured BrdU signal intensities of individual cell are plotted in the graphs as Z-height (**B, E**). The insets show magnified DIC images of GFP-expressing cells.

Supplementary Figure 9

Sweating response is detectable in melanocyte-deficient *Kit$^{W/W\text{-}V}$* mice

A-D, Representative images of footpad skin from sweating assays. Sweating was induced in 3 week-old mice by treatment with 2 mg/mL pilocarpine, a muscarinic receptor agonist, and visualized with iodine-starch reagent. The footpad of *Kit$^{W/W\text{-}V}$* mice (**C**, **D**) shows a comparable response to wild-type mice (**A**,**B**).

Supplementary Figure 10

Low level of MART1 is expressed by quiescent McSC-like cells in human hair follicles.

A-I, Immunofluorescent staining of the hair follicles of human scalp skin using anti-MART1 antibody with and without the tyramide amplification method for sensitive detection of the melanocyte lineage marker MART1. With the ordinary immunostaining method, MART1 expression was not found in the bulge area (**A**). By using signal amplification with tyramide, quiescent MART1^{low} melanoblasts (green) were clearly detectable in the bulge are of hair follicles which grow pigmented hair (**B**: arrow) but not of those which grow unpigmented hair (**C**). The signal specificity was confirmed by the absence of any signals in the bulb in non-pigmented hair follicles (**D-I**). Quiescent cells were detected by the absence of the expression of MCM2 (blue). The inset shows a magnified image of MART1 expressing McSC-like cell.

Supplementary Figure 11

Human MART1$^+$ melanoblasts are located in the epidermis and SP of sweat gland in the acral skin.

A-F, MART1^{+} melanoblasts (arrows) are located in the SP area (C and F) in sweat glands (but are not detected in duct areas (B and E)) in human infant (A, B and C) and adult (D, E and F) skin. The inset shows a magnified image of MART1 expressing cells.

Supplementary Figure 12

Expression of most melanogenic proteins is undetectable in human melanoblasts in the SP of sweat glands in infant skin.

Immunofluorescent staining of human infant acral skin showed that expression of Dct (**A**: green), MITF (**B**: green), NKIbeteβ (**C**: green), HMB45 (**D**: green), TYR (**E**: green), and c-kit (**F**: red) positive cells (arrow) were found only in the epidermis, but not in the ducts or in the SP (**G - R**). Nuclei are counterstained with DAPI (blue). The insets show magnified images of melanocytes in the epidermis. c-Kit expression was found also in glandular cells in the SP (**R**: red: dotted arrows).

Supplementary Figure 13

Human melanoblasts in the SP of sweat glands do not express HMB45, TYR, or Ki67 in adult skin.

Immunohistochemical staining of human adult acral skin showed that HMB45 (**A**: brown) and TYR (**B**rown) positive cells (arrow) were found only in the epidermis, but not in the ducts or in the SP (**C - F**). Nuclei are counterstained with Hematoxylin (violet). The insets show magnified images of melanocytes in the epidermis.

G, Immunofluorescent staining showed that MART1 (green) positive cells (arrow) are kept quiescent, as shown by the absence of Ki67 expression (red), both in the epidermis and in the SP in the sweat gland. KI67+ expression was confined to MART1- keratinocytes (arrowhead). Nuclei were counterstained with DAPI (blue). The insets show magnified images of MART1+ cells. The mark "*" indicates the deposition of fluorescent material aggregates was often found in the SP, which can be discriminated by the non-cellular shaped pattern.

Supplementary Figure 14

Hypothetical scheme of melanomagenesis in human acral skin.

In normal acral skin, McSC-like cells are kept within the SP of sweat glands in a quiescent and immature state (shown in the upper scheme). Upon activation by genotoxic stress, they transiently renew themselves within the niche. During early melanomagenesis, a McSC-like cell in a particular sweat gland is stably activated by *CCND1* gene amplification and transformed into a melanoma-initiating McSC-like cell to keep providing progeny that migrate upward through the duct and spread into the epidermis. In early acral melanoma *in situ* (shown in the lower

scheme), amplifying progeny of melanoma-initiating McSC-like cells spread horizontally within the epidermis and become preferentially distributed and produce melanin in the ridge epidermis (CPI of the epidermis). The McSC-like cells behavior may explain why acral melanomas show a "parallel ridge pattern" of skin hyperpigmentation which is seen preferentially around the opening of sweat glands.

Supplementary Material and Methods

Animals

Dct-lacZ transgenic mice were previously described(Mackenzie et al., 1997; Nishimura et al., 2002) (a gift from Dr. Ian J. Jackson, MRC, U.K.). *Mitf-ce* mice were a kind gift from Dr. M. Lynn Lamoreux(Zimring et al., 1996). Crossing to *Dct-H2B-GFP* transgenic mice and subsequent breeding was performed as previously described(Inomata et al., 2009; Nishimura et al., 2005) $Kit^{W/W\text{-}V}$ mice were purchased from Japan-SLC (Shizuoka, Japan). Animal care was in accordance with the Guidance of Kanazawa University and the Tokyo Medical and Dental University for Animal and Recombinant DNA Experiments. All animal experiments were performed following the Guidelines for the Care and Use of Laboratory Animals, and were approved by the Institutional Committee of Laboratory Animal Experimentation (Research Institute for Kanazawa University and Tokyo Medical and Dental University). Offspring were genotyped by PCR-based assays of mouse-tail DNA.

Generation of transgenic mice

To generate melanocyte lineage specific expression vectors for mH2B-EGFP (pDct-H2B-GFP-bGHpA) (Dct-H2B-GFP ver.1), the coding sequences for mH2B were PCR amplified using LA-Taq (Takara, Shiga, Japan) from mouse ES cell cDNA libraries. The primers used are as follows (restriction enzyme sites are underlined, kozaq sequences are shown as bold characters): for mouse H2B, 5'-CGGGAATTC**GCCACC**ATGCCTGAGCCTGCGAAGTCC-3' and 5'-CGGCTCGAGGCCGCCCTTGGCGCTAGTATACTTGT-3'. The PCR products were digested with EcoRI and XhoI, and cloned into pPyCAGIP-EGFP–N. Next, the H2B-GFP fusion gene was PCR amplified. The primers used are as follows (restriction enzyme sites are underlined): for H2B-GFP, 5'-GAAGGCTCCCAATTAAGAAGGC GCCACCATGCCTGAGCCTGCGAAGTCC-3' and 5'-GCC GAATTCTAACTTGTACAGCTCGTCCATGCC -3'. The PCR products were digested with StuI and EcoRI. A fragment containing bovine growth hormone polyA (bGHpA), which has been shown to increase the translation of reporter transgenes(Pfarr et al., 1986), was obtained from

pTRP2-TVA (a kind gift from Dr. Mariko Moriyama, Dr. Masatake Osawa and Dr.. Shinichi Nishikawa, RIKEN CDB). The SCS110 amplified pTRP2-TVA unmethylated plasmid was digested with Stu1 and Xba1. Finally, the 3 fragments were ligated and the pDct-H2B-GFP-bGHpA vector was obtained.

For the generation of Dct-H2B-GFP ver.2, the three PCR-amplified fragments encoding TYR-LCR, pDct-H2B-gfp-bGHpA and the pUC18 backbone including the Amp resistant gene and replication origin, were used. PCR reaction was performed with Primestar GXL (Takara, Shiga, Japan) with 15~20 cycles to avoid mismatched nucleotide incorporation. Primers used are as follows (restriction enzyme sites are underlined). For pDct-H2B-gfp-bGHpA, 5'-ATAAGAATGCGGCCGCAATGAGATGACAGCGGGTAAAGAAGCCTA-3' and 5'-CTAGCTAGCGCCATAGAGCCCACCGCATCCCCAG-3'; for TYR-LCR, 5'-AGGGATCCGAATTCTGTCCTAAAACAGTCTTTG-3' and 5'-ATAAGAATGCGGCCGCGAATTCATGCCGTTAAGCTTGATAG-3'; for the pUC19 backbone, 5'-CTAGCTAGCAACATACGAGCCGGAAGCATAAAG-3' and 5'-AGGGATCCGACGTCAGGTGGCACTTTTCG-3'. The PCR products were digested with NotI, Nhe1, BamH1, and were ligated. For the large size (approx. 10.5 kbp) construct encoding Dct-H2B-GFP-pA ver.2, we used HTS02 competent cells (Takara, Shiga, Japan) to obtain transformed clones, and these were usually maintained in this line to prevent undesired recombination. All sequences of the clones were checked using Big Dye terminator v1.1 equipped with ABI 3100-Avant (Life Technologies, CA, U.S.A.). The linearized transgene excised from the E. coli derived plasmid sequence was injected into fertilized oocytes of C57BL/6J mice. Transgenic founders were identified by PCR analysis of tail DNA or direct fluorescent signals from a piece of cut ear skin. Primers corresponding to GFP coding regions are as follows: 5'-TCGTGAACGACATCTTCGAG-3' and 5'-GAACTTCAGGGTCAGCTTGC-3'. Established transgenic lines were maintained by breeding to non-transgenic C57BL/6J mice. Unless noted, we mainly utilized *Dct-H2B-GFP* ver.2 tg mice as *Dct-H2B-GFP* tg mice, because these mice show consistently strong signals.

Total Skin X-ray irradiation of mice

Total skin X-ray irradiation (IR) was performed using a Hitachi MBR-1520 (Hitachi Medical, Tokyo, Japan) or RX-650 (Faxitron X-Ray, Lincolnshire, IL, USA). Irradiation was done at the dose of 5 Gy using Aluminum filters as previously described(Inomata et al., 2009). Irradiation was carried out by placing the mice in a thin-walled plastic box.

UV irradiation and DMBA treatment of mice

UV irradiation was performed using a Y-UV-Lab-K-D (YAYOI. CO. LTD., Tokyo, Japan).

Irradiation was performed 3 times per week at a dose of 200 J/m^2 as previously reported(Takeuchi et al., 2004). The average output of the UVB lamps during the experiment was as follows: UVA, 39.7 %; UVB, 60.2%; and UVC, 0.1%. DMBA dissolved in acetone solution, was topically applied to the footpad, once per week, at the dose of 100 μg/ml(Abel et al., 2009).

ACK2 preparation

A rat monoclonal antibody against the c-kit receptor protein (ACK2) was prepared as previously described(Nishimura et al., 2002).

Sweating test

The iodine-starch sweating test was performed as previously reported(Cui et al., 2012). Briefly, 0.2mg/mL iodine (Sigma, MO, U.S.A.) in Ethanol was applied to a hindfoot sole skin of the mouse. After drying, the surface of the skin was painted with 1g/mL cornstarch in castor oil (Sigma, MO, U.S.A.).

Sciatic denervation of mice

The sciatic denervation was performed in the left hind limb over the pelvic joint of 7 week old mice, as previously described(Grant et al., 1991). An 8-10 mm segment of the sciatic nerve, exposed from the incised muscle fascia between the vastus lateralis and the biceps femoris, was removed, and then the incision was closed with wound clips. The right hind limb of each mouse was sham-operation treated, and was used as a control.

Whole mount histochemical detection of β-galactosidase staining

Skin samples from *Dct-lacZ* transgenic mice or whole embryos (E13.5-16.5) were immersed in fixation solution (2% formaldehyde, 0.2% glutaraldehyde, 0.02% Nonidet P-40 in phosphate-buffered saline (PBS), pH 7.4), irradiated for 30 sec in a 500W microwave oven at 4°C and kept on ice for 20-30 min. The fixed samples were stained in 5-bromo-4-chloro-3-indolyl-B-D-galactosidase (X-gal) (Life Technologies, CA, U.S.A.) solution overnight. The stained tissues were subjected to post-fixation with 10% formalin in PBS (pH 7.4) and images were captured with a SZX12 microscope (Olympus, Tokyo, Japan)-mounted digital camera. The stained tissues were embedded in paraffin and the specimens were cut into 5 μm-thick sections (Rotary Microtome HM325, MICROM International GmbH., Walldorf, Germany). The sections were deparaffinized, rehydrated, and stained with hematoxylin-eosin (Sakura Fine technical Co. Ltd., Tokyo, Japan) with/without Fontana-Masson silver stain (Diagnostic BioSystems, Pleasanton, CA, USA). Coverslips were mounted onto glass slides with

mounting media MOUNT-QUICK (Daidosangyo Co., Ltd., Tokyo, Japan) or Soft-mount (Wako Chemicals, Osaka, Japan). Images were captured with an upright microscope BX51 (Olympus, Tokyo, Japan).

GFP imaging of whole embryos

PBS-washed embryos (E14.5) were immersed in ice-cold 4% paraformaldehyde (PFA) in PBS, and were irradiated in a 500W microwave oven for 30 sec 3 times with 1 min intervals. After washing with PBS, each embryo was gently mounted on a glass slide with a coverslip, and fluorescence was imaged using an upright microscope BX51 (Olympus, Tokyo, Japan).

Immunofluorescence and immunohistochemistry

Pieces of fresh mouse skin were immersed in ice-cold 4% PFA in PBS, and were irradiated in a 500W microwave oven for 30 sec 3 times. The fixed skin samples were embedded in OCT compound (Sakura Fine technical Co. Ltd., Tokyo, Japan), snap-frozen in liquid nitrogen, and stored at –80°C. Human fresh skin samples were obtained from surgical specimens as a therapy of polydactyly patients in accordance with consent procedures approved by the Institutional Review Board of the National Center for Child Health and Development. Fresh OCT-embedded human samples were snap-frozen in liquid nitrogen and were stored at –80°C until used. Formalin-fixed human melanoma samples were embedded in paraffin, and the specimens were cut into 5 μm-thick sections that were subsequently deparaffinized and rehydrated before use. Frozen samples of mouse tissues were cut into 10 μm-thick sections (Cryomicrotome CM 1850, Leica Microsystems, HESSEN Wetzlar, Germany), and were used for immunofluorescence analysis. For human frozen skin sections, 10 μm-thick sections were post-fixed with 4% PFA. Antigen retrieval of paraffin sections was performed using citrate buffer, pH 6.0, at 90°C for 20 min. Nonspecific staining was blocked by incubation with Tris-buffered saline/0.1% Tween-20 (TBST) containing 0.3% skim milk and 0.1% Triton X-100 for 30 min. Endogenous peroxidase activity was quenched by incubation in 0.15% H_2O_2 in TBST for 10 min. For the detection of BrdU, 2M HCl incubations were done before applying antibodies. Tissue sections were incubated with the primary antibody at 4°C overnight, and were subsequently incubated with appropriate secondary antibodies conjugated with Alexa Fluor 488, 568 or 594 (Life Technologies, CA, U.S.A.) for immunofluorescence. For the staining of MART1 in human skin samples, tyramide-amplification (for immunofluorescence) or polymer-based amplification (for immunohistochemistry) was performed using a TSA-plus FITC kit (Perkin Elmer) or Envision G2 system (DAKO, Copenhagen, Denmark). After washing in TBST, 4', 6-diamidine-2'-phenylindole dihydrochloride (DAPI, Life Technologies, CA, U.S.A.) was added for nuclear counterstaining for immunofluorescence. For immunohistochemistry, nuclei were

counterstained with hematoxylin. Coverslips were mounted on glass slides with fluorescent mounting medium Permafluor (Thermofisher Scientific, MA, U.S.A.) or with Softmount (Wako, Osaka, Japan). All images were obtained using an upright microscope BX51 (Olympus, Tokyo, Japan) or a FV1000 confocal microscope system (Olympus, Tokyo, Japan).

FISH Analysis

Gene amplification of the *CCND1* gene (11q13) was analyzed in paraffin-embedded tissue sections with a dual-color FISH technique as previously described(Yamaura et al., 2005). A dual-color probe mixture consisting of a Spectrum Orange LSI CCND1 probe and Spectrum Green CEP 11 probe was purchased from Abbott Japan, Tokyo, Japan. Briefly, paraffin-embedded tissues were cut into 4 μm sections, and mounted on MAS coated slides (Matsunami, Osaka, Japan). FISH signals were analyzed with a FV1000 confocal microscope. Copy numbers of CEP11 (green) and CCND1 signals (red) were, respectively, counted for more than 30 non-overlapping tumor cells in each region.

Antibodies

For immunofluorescence and immunohistochemistry, the following antibodies were used: rabbit anti-MCM2 (1:200, Abcam, Cambridge, U.K.), rat clone A5 anti-LaminB2/γ1 (1:30, Thermofisher Scientific, MA, U.S.A.), rat clone ACK45 anti-c-Kit antibody (1:200, BD Pharmingen, NJ, U.S.A.), mouse clone D5 anti-MITF (1:5), mouse anti-Pax3 (1:100, Developmental Studies Hybridoma Bank, IA, U.S.A.), rat clone BU1/75 (ICR-1) anti-BrdU (1:200, Abcam, Cambridge, U.K.), rabbit anti-Ki67 (1:200, Novocastre Laboratories, Newcastle, U.K.), chicken anti-Nestin (1:2000, Aves labs, OR, U.S.A.), rabbit anti-p75 (1:100, Millipore, MA, U.S.A.), rabbit anti-Neuronal Class III β-Tubulin (TuJ1)(1:2000, Covance, NJ, U.S.A.), rabbit anti-keratin 5 (1:2000, Covance, NJ, U.S.A.), rabbit anti-γH2AX (1:100, Cell signaling, MA, U.S.A.), rabbit anti-Glial Fibrillary Acidic Protein (1:1000, DAKO, Copenhagen, Denmark), chicken anti-Myelin Protein Zero (1:100, Novus Biologicals, CO, U.S.A.), rabbit anti-Ubiquitin Carboxyl-terminal Esterase L1 (PGP9.5) (1:300, Lifespan BioSciences, WA, U.S.A), rabbit anti-alpha smooth muscle actin (aSMA) (1:500, Abcam, Cambridge, U.K.), rat anti-cytokeratin Endo-A (Keratin 8) (1:200, Developmental Studies Hybridoma Bank, IA, U.S.A.)), goat anti-Dct (1:100, Santa Cruz, CA, U.S.A.), mouse anti-NKI/beteβ (1:10, Abcam, Cambridge, U.K.), mouse clone HMB45 anti-gp100 (1:50, DAKO, Copenhagen, Denmark), mouse clone T311 anti-tyrosinase (1:50, Abcam, Cambridge, U.K.) and mouse anti-MART1 cocktail (1:100 (paraffin) ~1:1000 (frozen), Thermofisher Scientific, MA, U.S.A.). Rabbit anti-TRP1 (PEP1) (1:1000), rabbit anti-Tyrosinase (PEP7) (1:1000) and rabbit anti-Pmel17 (PEP13)(1:1000) were kind gifts from Dr. Vincent Hearing, National Cancer Institute(Jiménez et al., 1989; Kobayashi

et al., 1994). Mouse anti-MITF (D5) (non-diluted) was a kind gift from Dr. David Fisher, Harvard Medical School(Wu et al., 2000).

Ethics statement

Human skin samples were collected from surgical specimens, under signed informed consent, with ethical approval of the Institutional Review Board of the National Institute for Child Health and Development and Shinshu University School of Medicine, Japan. Signed informed consent was obtained from each donor, and the surgical specimens were de-identified. All experiments handling human tissues were performed in line with Tenets of the Declaration of Helsinki.

Quantification of McSC number and Statical analysis

To obtain the exact number of McSCs in each eccrine gland of mice, we cut out all sections from a single hindfoot of mice, and counted the total number of $GFP^{+}TuJ1^{-}$ cells existing within eccrine glands from one hindfoot (usually 30-40 x 10 um sections per foot). Since one hindfoot contains 6 footpads, which contains several eccrine glands unit per footpad. This is how we obtained the McSC number in a single footpad. Statistically significant differences in the parameters tested were determined by applying Student t test statistics to the obtained experimental data. The obtained data was basically from the three or more mouse, otherwise indicated, and the number of independent experiments is indicated in the respective figure legend.

Supplementary References

Abel, E. L., Angel, J. M., Kiguchi, K., and DiGiovanni, J. (2009). Multi-stage chemical carcinogenesis in mouse skin: Fundamentals and applications. Nat Protocols *4*, 1350-1362.

Cui, C.-Y., Childress, V., Piao, Y., Michel, M., Johnson, A. A., Kunisada, M., Ko, M. S. H., Kaestner, K. H., Marmorstein, A. D., and Schlessinger, D. (2012). Forkhead transcription factor FoxA1 regulates sweat secretion through Bestrophin 2 anion channel and Na-K-Cl cotransporter 1. Proceedings of the National Academy of Sciences *109*, 1199-1203.

Grant, M., Landis, S., and Siegel, R. (1991). The molecular and pharmacological properties of muscarinic cholinergic receptors expressed by rat sweat glands are unaltered by denervation. The Journal of Neuroscience *11*, 3763-3771.

Inomata, K., Aoto, T., Binh, N. T., Okamoto, N., Tanimura, S., Wakayama, T., Iseki, S., Hara, E., Masunaga, T., Shimizu, H., and Nishimura, E. K. (2009). Genotoxic Stress Abrogates Renewal of Melanocyte Stem Cells by Triggering Their Differentiation. Cell *137*, 1088-1099.

Jiménez, M., Maloy, W. L., and Hearing, V. J. (1989). Specific identification of an authentic clone for mammalian tyrosinase. Journal of Biological Chemistry *264*, 3397-3403.

Kobayashi, T., Urabe, K., Orlow, S. J., Higashi, K., Imokawa, G., Kwon, B. S., Potterf, B., and Hearing, V. J. (1994). The Pmel 17/silver locus protein. Characterization and investigation of its melanogenic function. Journal of Biological Chemistry *269*, 29198-29205.

Mackenzie, M. A. F., Jordan, S. A., Budd, P. S., and Jackson, I. J. (1997). Activation of the Receptor Tyrosine Kinase Kit Is Required for the Proliferation of Melanoblasts in the Mouse Embryo. Developmental Biology *192*, 99-107.

Nishimura, E. K., Granter, S. R., and Fisher, D. E. (2005). Mechanisms of Hair Graying: Incomplete Melanocyte Stem Cell Maintenance in the Niche. Science *307*, 720-724.

Nishimura, E. K., Jordan, S. A., Oshima, H., Yoshida, H., Osawa, M., Moriyama, M., Jackson, I. J., Barrandon, Y., Miyachi, Y., and Nishikawa, S.-I. (2002). Dominant role of the niche in melanocyte stem-cell fate determination. Nature *416*, 854-860.

Pfarr, D. S., Rieser, L. A., Woychik, R. P., Rottman, F. M., Rosenberg, M., and Reff, M. E. (1986). Differential effects of polyadenylation regions on gene expression in mammalian cells. DNA *5*, 115-122.

Takeuchi, S., Zhang, W., Wakamatsu, K., Ito, S., Hearing, V. J., Kraemer, K. H., and Brash, D. E. (2004). Melanin acts as a potent UVB photosensitizer to cause an atypical mode of cell death in murine skin. Proceedings of the National Academy of Sciences of the United States of America *101*, 15076-15081.

Wu, M., Hemesath, T. J., Takemoto, C. M., Horstmann, M. A., Wells, A. G., Price, E. R., Fisher, D. Z., and Fisher, D. E. (2000). c-Kit triggers dual phosphorylations, which couple activation and degradation of the essential melanocyte factor Mi. Genes & Development *14*, 301-312.

Yamaura, M., Takata, M., Miyazaki, A., and Saida, T. (2005). Specific Dermoscopy Patterns and Amplifications of the Cyclin D1 Gene to Define Histopathologically Unrecognizable Early Lesions of Acral Melanoma In Situ. Arch Dermatol *141*, 1413-1418.

Zimring, D. C., Lamoreux, M. L., Millichamp, N. J., and Skow, L. C. (1996). Microphthalmia cloudy-eye (mi(ce)): a new murine allele. J Hered *87*, 334-338.